Energy Policy 89 (2016) 311–329

Contents lists available at ScienceDirect

Energy Policy

journal homepage: www.elsevier.com/locate/enpol

Electric power grid interconnections in Northeast Asia: A quantitative analysis of opportunities and challenges

Takashi Otsuki [a,*], Aishah Binti Mohd Isa [b,1], Ralph D. Samuelson [c,1]

[a] Asia Pacific Energy Research Centre (APERC), The Institute of Energy Economics, Japan (IEEJ), Inui Bldg.-Kachidoki 11F, 1-13-1 Kachidoki, Chuo-ku, Tokyo 104-0054, Japan
[b] College of Engineering, Universiti Tenaga Nasional, Jalan IKRAM-UNITEN, 43000 Kajang, Selangor, Malaysia
[c] Ministry of Transport, Level 6 SAS House, 89 The Terrace, Wellington 6011, New Zealand

HIGHLIGHTS

- We developed a multi-region power system model of Northeast Asia (NEA).
- The model considers renewable energy in the Gobi Desert and eastern Russia.
- Expanding renewables for export brings CO_2 reductions and fuel cost savings in NEA.
- Economic benefits due to reduced total costs are modest.

ARTICLE INFO

Article history:
Received 25 March 2015
Received in revised form
4 October 2015
Accepted 21 November 2015
Available online 18 December 2015

Keywords:
Grid interconnections
Electricity trade
Renewable energy
Northeast Asia
Linear programming
Energy systems modeling

ABSTRACT

Power grid interconnection has gained attention in Northeast Asia (NEA) as a means to build an economically efficient power system and to effectively utilize renewable energy, such as wind and solar resources in the Gobi Desert and hydro resources in Eastern Russia.

In order to quantify the potential economic and environmental benefits from connecting power grids and developing renewables in NEA, we build an NEA-wide multi-region power system model using linear programming techniques. Our analysis considers power system characteristics, such as the seasonal and daily electric load curves of the various NEA economies.

Compared to a "no grid extension" scenario, increased access to renewables contributes significantly to emissions reductions and fuel cost savings. However, the results imply modest benefits in lowering total cost because of the large initial investments needed in developing the renewables and the transmission lines. These limited total cost savings are likely to pose an implementation challenge for NEA grid interconnections. Our results also suggest that grid interconnections become more economically attractive in higher fuel price or lower initial cost situations. The relevant planning organizations should carefully consider the initial cost and future fuel price trends when considering how to interconnect power girds in an economical manner.

1. Introduction

Over the past two decades, electric power grid interconnections have gained attention in Northeast Asia (NEA), an area that we define as four Asia Pacific Economic Cooperation (APEC) economies—China, Japan, the Republic of Korea (Korea), and Russia—and two non-APEC economies—Mongolia and the Democratic People's Republic of Korea (DPRK). Various interconnection schemes have been proposed for NEA (Streets, 2003; Yun and Zhang, 2006; Hippel et al., 2011). Yet, while technically feasible, these cooperative proposals have been hampered by factors such as existing national policies of energy self-sufficiency and the sometimes-volatile diplomatic and political situation in the region. Thus, the only existing cross-border power cooperation projects are small in scale, linking Russia to Mongolia, Russia to China, and China to the DPRK.

However, several recent regional events, including the Fukushima nuclear disaster in Japan, the power shortage and rolling blackouts in Korea, and increased concern regarding air pollution in China, have made power grid interconnections potentially more

* Corresponding author.
E-mail address: takashi.otsuki@aperc.ieej.or.jp (T. Otsuki).
[1] Formerly Asia Pacific Energy Research Centre (APERC).

http://dx.doi.org/10.1016/j.enpol.2015.11.021

attractive. Several organizations have proposed multilateral power grid interconnection concepts in NEA, i.e., *Asia Super Grid (ASG)* and *Gobitec*, with a focus on developing the abundant renewable resources in the Gobi Desert and Eastern Russia and on building a more resilient and economically efficient power system (KEPCO, 2014; Energy Charter et al., 2014; Graaf and Sovacool, 2014). The wind and PV potential in Mongolia has been estimated at 1100 GW and 1500 GW, respectively (Elliott et al., 2001; Energy Charter et al., 2014), and economically feasible hydropower potential in Eastern Russia is estimated at 690 TWh/yr (estimated by European Bank for Reconstruction and Development, see IEA (2003)).

There have been some previous economic analyses on connecting power grids in various parts of the world: Southern Africa is the focus of Bowen et al. (1999), Europe of Lilliestam and Ellenbeck (2011) and Schaber et al. (2012) and Southeast Asia of Chang and Li (2013) and Matsuo et al. (2015). Among those studies, Schaber et al. (2012) conducted a detailed analysis on the impacts of grid interconnections on regional renewable energy utilization. They employed a Europe-wide power system model with a detailed temporal resolution (hourly time slice for six representative weeks), which appropriately reproduce the actual power generation, electricity prices and cross-border power transportation.

The economics of power grid interconnection in the NEA region have also been investigated. Cost–benefit analyses of grid interconnection scenarios in NEA were performed by Hippel (2001), Podkovalnikov (2002), Lee et al. (2005), Chung and Kim (2007), Energy Charter et al. (2014) and Skoltech (2015). Analyses of power system reliability were conducted by Choi et al. (2006) and Yoon (2007). Yet, to our knowledge, few studies have focused on the whole of NEA and analyzed the impacts of grid interconnections with a focus on renewables both in the Gobi Desert and Eastern Russia considering power system characteristics (e.g. load curves, generation dispatch). Except for Energy Charter et al. (2014) and Skoltech (2015), the studies listed above covered only a part of NEA (three to four out of the six economies) and did not consider renewable energy in the Gobi Desert. Skoltech (2015) also does not take into account renewables in the Gobi Desert. As for Energy Charter et al. (2014), they proposed to install 50 GW of wind and 50 GW of solar photovoltaics (PV) in the Gobi Desert, and estimated the supply costs to other NEA economies. However, their cost assessment did not consider regional power system characteristics, such as the load curves of the importing economies and the seasonal and diurnal output variation of the solar and wind power from the Gobi Desert.

Thus, we developed a multi-region power system model, which covers the whole of NEA, in order to quantitatively evaluate the potential benefits of, and barriers to, power grid interconnection and expansion of renewable energy for export. The model seeks to minimize overall system cost, considering seasonal and daily characteristics of electric load of each region and the output patterns of renewables in the Gobi Desert. This model can determine cost-optimal grid expansion and cross-boundary power flows, as well as generation dispatch. Also, nodal marginal pricing gives us some implications for regional electricity prices. We believe that our analysis contributes to understanding of the costs and benefits of grid interconnection and large-scale renewable energy utilization in NEA from a systems viewpoint.

This paper proceeds as follows: Section 2 gives an overview of the multi-region power system model and the scenario assumptions; Section 3 presents the simulation results and discusses the economic feasibility of grid interconnections, as well as a sensitivity analysis on initial cost and energy prices; and Section 4 summarizes major conclusions and implications, and then proposes a future research agenda.

2. Methods

2.1. Overview of the multi-region power system model

We developed a multi-region power system model using linear programming techniques. Fig. 1 is a schematic diagram of this model. The model aims to minimize a single-year overall system cost, consisting of the annualized initial cost, operation and maintenance (O&M) cost, fuel cost and carbon cost for the whole NEA under various technical and political constraints. Hence, the NEA economies are assumed to cooperate fully to achieve the regional optimization. A detailed mathematical description of the model is provided in Appendix A.1. Validation of the model is discussed in Appendix A.2.

A capital recovery factor is used to annualize initial investments in generation, storage and cross-boundary transmission facilities. The assumed discount rate is 3% and lifetime assumptions are discussed in Sections 2.3.2 and 2.3.5. O&M cost includes both fixed and variable O&M cost. Fixed O&M cost, which is incurred even if the plant is not operated (i.e., landowner cost), is assumed to be in proportion to capacity, while variable O&M cost (i.e., consumables) varies with generated electricity. Carbon cost in this study considers only direct emissions from fuel combustion.

The cost of generation includes initial cost, fixed and variable O&M cost, fuel cost and carbon cost. The cost of cross-boundary transmission lines includes initial cost and fixed O&M cost. Power trade is selected by the model if its benefit (usually the savings in generation cost) is larger than the cost of cross-boundary transmission lines.

This model is formulated in a consistent way in General Algebraic Modeling System (GAMS) software. There are 75,000 equations or constraints and 38,000 endogenous variables. For our modeling work, we referred to the detailed modeling approach in Schaber et al. (2012), Komiyama and Fujii (2014) and Komiyama et al. (2015), but due to data availability we selected the temporal and geographical resolution explained below.

Regarding the temporal resolution, the model considers the hourly load curves of typical days for five seasons (Summer-peak, Summer-average, Winter-peak, Winter-average, and Intermediate) in order to model the diversity of seasonal and daily load variation among the regions. Thus, in each node, one calendar year is decomposed into 120 time segments ($=24$ h per day $\times 1$ representative day per season $\times 5$ seasons per year).

As for the geographical resolution, we divide NEA into ten nodes (Fig. 2), represented by seven city nodes (round markers) and three supply nodes (triangle markers). City nodes have electricity demand and power supply facilities, while supply nodes have only power supply facilities to export electricity. Endogenous capacity additions are allowed in both types of nodes. Five of the city nodes correspond to power grids or power service areas: North China grid (CH-N); China Northeast grid (CH-NE); Japan Hokkaido area (JP-H); Korea (KR), and Russia Far East power

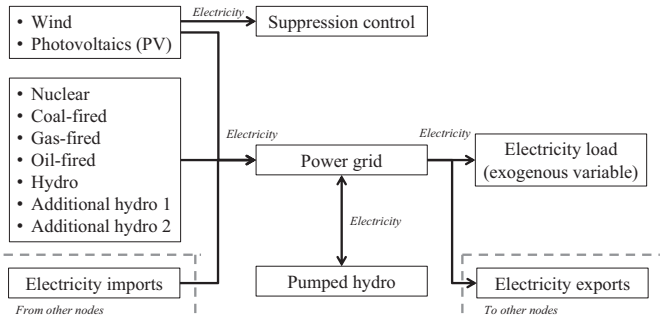

Fig. 1. Schematic diagram of the multi-region power system model.

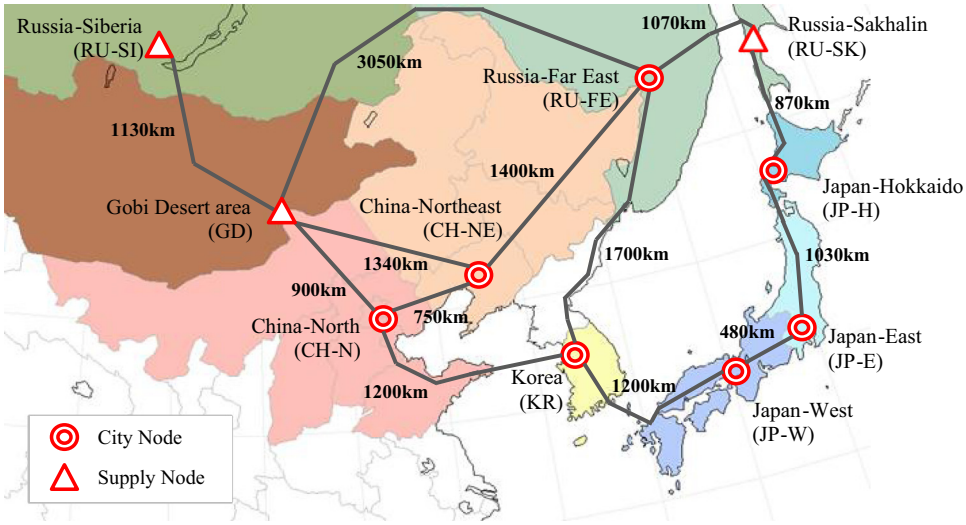

Fig. 2. Regional division and assumed transmission distances.

Table 1
Definition of scenarios.

Scenario	*Base*	*NoNewRE*	*RuHyd*	*Gobitec*	*Gobitec+RuHyd*
Fossil fuel fired capacity	Cost optimized for all scenarios. For coal-fired plants, we impose upper bounds based on the projected capacity in APERC (2013), reflecting environmental concerns.				
Wind/PV Capacity	Projected capacity for 2030 for the *Base*, *NoNewRE* and *RuHyd* scenarios (APERC, 2013)			Gobi desert (GD): 50GW solar, 50 GW wind (Energy Charter, et al., 2014). Other nodes: same as *Base* scenario	
Hydro Capacity	Projected capacity for 2030 (APERC, 2013)		Endogenous additions allowed in Russia nodes for export (see Section 2.3). Other nodes: same as *Base* scenario	Same as *Base* scenario	Same as *RuHyd* scenario
Interconnection	Current capacity	Cost optimized for the last four scenarios			
Carbon price	30$/t-$CO_2$ for all scenarios				

system (RU-FE). The Tohoku and Tokyo areas in Japan are aggregated as JP-E, and the western parts of Japan as JP-W. Supply nodes consist of the Gobi Desert area in Mongolia (GD), the Russia Siberia area (RU-SI) and the Russia Sakhalin area (RU-SK), which have abundant energy supply potential (wind and solar in GD, hydro in RU-SI and coal and gas in RU-SK). Assumptions for these nodes are discussed in Section 2.3.

We modeled electricity transmission as a transport problem. Kirchhoff's first law (conservation of current) is considered in each node of the network, but the second law (voltage law) is not incorporated. This simplified approach allows us to keep the optimization problem linear and to optimize grid extensions, generation expansion and their operations simultaneously (Schaber et al., 2012). Distances between nodes in Fig. 2 were based on airline distances between representative cities in each region plus 20% to allow for expected circuity (Google, 2015; Energy Charter et al., 2014). Regarding the transmission between KR and RU-FE, there are significant diplomatic challenges involved in arranging transit across the DPRK. However, we take this route into account as the Korea Energy Master Plan explicitly mentions that the connection "should be a prospective mid- to long-term governmental project" if it is profitable and overall conditions, including inter-Korean relations, improve (MOTIE, 2014).

2.2. Scenario setup

We examine the five scenarios in Table 1. The simulated year in this study is 2030. The *Base* scenario assumes no grid expansion from the existing transmission line capacity. In the *NoNewRE* scenario, new interconnections are allowed based on total system cost optimization, but renewable capacity is fixed to the *Base* scenario assumptions at all nodes. The *RuHyd* scenario endogenously allows additional hydro power development in the Russian nodes. As hydro power development for Russian domestic supply is already considered in the initial capacity settings (APERC, 2013), we assume that the additional hydro plants are used only for exports to the foreign nodes in this study. The *Gobitec* scenario attempts to quantify the costs and benefits of the "*Gobitec/ASG*" concept proposed by Energy Charter et al. (2014). They targeted 50 GW wind and 50 GW solar PV[2] in GD (the Gobi Desert) by 2030, although we believe sensitivity analyses on the capacity needs to be considered in future work. The last scenario (*Gobitec+RuHyd*)

[2] To our knowledge, they do not mention the reason for their choice of this level of capacity, yet there seems to be a consideration of energy security risks (Mano, 2014). The land area of 50 GW solar PV capacity would account for approximately 0.1% of the Gobi Desert, assuming that total Gobi Desert area is 1,300,000 km^2 and the land area required for solar PV cells is 20 km^2/GW (Eurus Energy, 2012).

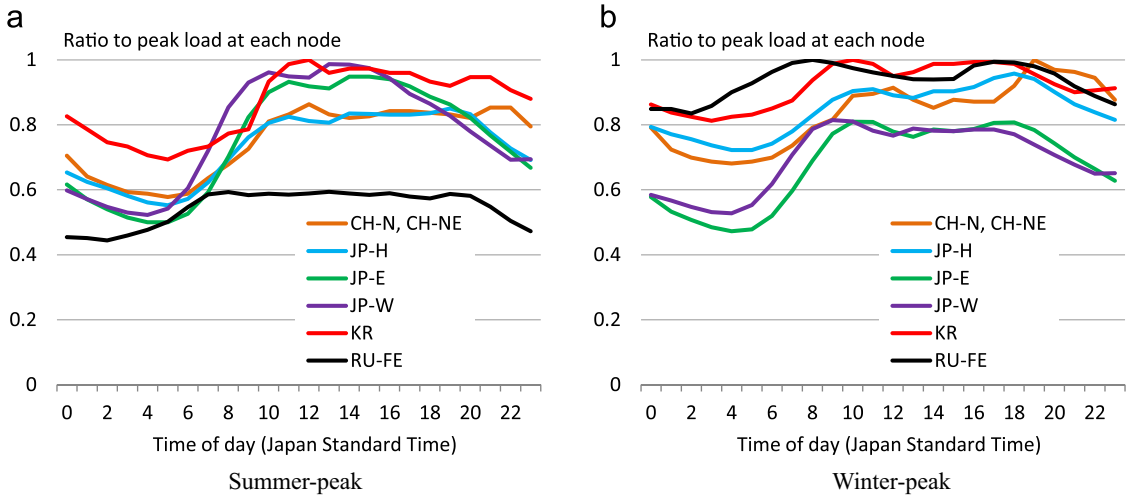

Fig. 3. Estimated electric load curve at city nodes in the summer-peak and winter-peak seasons (ratio to peak load at each node).

considers both the *Gobitec* and the *RuHyd* assumptions. The assumed carbon price for all scenarios is 30$/t-$CO_2$. Further explanations of the assumptions, including the limits for fossil fuel capacity additions and additional hydro potentials in Russia, are given in Section 2.3.

Kunstýř and Mano (2013) investigated the security risks for Japan of importing electricity from Russia. They concluded that the power trade would not pose substantial security risks for Japan with the appropriate measures, such as ensuring a capacity buffer at the current level. In general, each service area needs to be prepared for cross-boundary transmission interruptions. Therefore we limit the share of net transmission inflows at each city node to be less than the reserve margin level as described in Eq. (A.26) in Appendix A.1. Note that Eq. (A.26) does not distinguish between transmission inflows from foreign and domestic sources, since either one can fail. This is especially true in the case of Japan, where the two domestic links represented in the model are technically similar to import links. The JP-H to JP-E link is an undersea DC connection. The JP-W to JP-E link is a back-to-back AC-to-DC-to-AC converter, similar to an undersea connection, due to the differing frequencies between JP-E (50 Hz) and JP-W (60 Hz).

2.3. Input data assumptions

2.3.1. Electricity demand and load curves

Our analysis considers the seasonal and diurnal characteristics of electric load in each node. We estimated electricity demand in 2030 from each node's historical data (JEPIC, 2013; Government of Japan, 2014) and the projected growth rate from APERC (2013). We also constructed daily load curves for the five seasons from available historical load curve information and load factor data (JEPIC, 2006; SO UPS, 2014; Government of Japan, 2014; Nagayama, 2014; JEPIC, 2014). Fig. 3 depicts the estimated daily load curves in the summer-peak and winter-peak seasons.[3] Note that all the curves are plotted in Japan Standard Time. Time differences among the modeled city nodes are a maximum two hours.[4] Japan and Korea are located in the same time zone. Compared to these two regions, China is one hour behind, while the Russia Far East area (Vladivostok time) is one hour ahead. The peak load season varies by node; for example, the peak load season is summer in JP-E and winter in RU-FE.

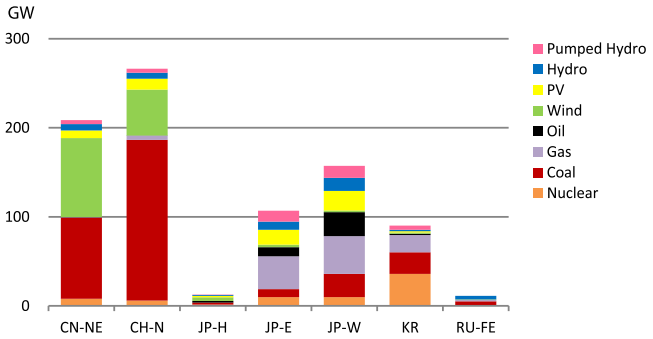

Fig. 4. Initial capacity settings of generation and storage facilities at city nodes.

2.3.2. Generation and storage facilities

The model is allowed to endogenously add fossil fuel-fired generation capacity in the all scenarios. Capacities for nuclear, solar PV, wind and pumped hydro are given exogenously in each scenario. Hydro plant capacities are exogenous variables, except for RU-SI and RU-FE in the *Ruhyd* and *Gobitec+RuHyd* scenarios. Assumptions for additional hydro potential for these nodes are discussed in Section 2.3.4. Fig. 4 depicts initial capacity settings for generation and storage facilities. The initial capacity of fossil fuel-fired plants and pumped hydro are based on existing capacities in 2011 (JEPIC, 2014; Hippel et al., 2011). For coal-fired plants, we impose upper bounds based on the projected capacity in APERC (2013), reflecting environmental concerns. The initial capacity for renewables, except for GD (the Gobi Desert area), is estimated based on the projected capacity for 2030 in APERC (2013) as well as renewable energy potential information (McElroy et al., 2009; Energy and Environment Council, 2011). For renewables in GD in the *Gobitec* and the *Gobitec+RuHyd* scenarios, we assumed 50 GW of PV and 50 GW of wind turbines (Energy Charter et al., 2014). For nuclear, we estimated capacity in 2030 based on available information (JAIF, 2013, 2014; MOTIE, 2014). Nuclear capacity in Japan assumes no new additions by 2030 and a 40-year lifetime for existing plants. We assumed that all remaining nuclear plants are restarted by the year 2030.

Tables 2–6 show the assumptions for generation and storage facilities. We set the assumptions in a consistent way, comparing

[3] Due to data availability, the same load curve is assumed for CH-N and CH-NE.

[4] None of the modeled city nodes in China, Japan, Korea and Russia use daylight saving time (DST) as of September 2015. Mongolia does use DST, but the wind and solar output curves in Figs. 6 and 7, as well as all of our other calculations for the Gobi Desert (GD), are in Mongolia Standard Time, which is the same as the time at the China nodes.

Table 2
Assumptions for generation and storage facilities.

	Nuclear	Coal	Gas	Oil	Hydro	Wind	PV	Pumped
Life time [year]	40	40	40	40	60	20	20	60
Carbon content [t-CO_2/toe]	0	3.80	2.07	2.86	0	0	0	0
Own-use rate [%]	4	6	3	5	–	–	–	–
Maximum ramp-up/down rate [%/h]	0	30	50	100	–	–	–	–
Capacity credit [%]	90	90	90	90	40	25	15	85
Minimum output level [%]	100	30	20	15	–	–	–	–
Cycle efficiency (storage) [%]	–	–	–	–	–	–	–	75
Self-discharge rate (storage) [%/h]	–	–	–	–	–	–	–	0.01
Maximum kWh ratio to kW (storage)	–	–	–	–	–	–	–	8

Table 3
Cost assumptions for North China (CH-N), China Northeast (CH-NE) and the Gobi Desert area (GD).

	Nuclear	Coal	Gas	Oil	Hydro	Wind	PV	Pumped
Initial cost [$/kW]	2600	750	700	800	2500	1300	1100	2500
Fixed O&M cost [$/kW/yr]	65	15	14	16	30	33	17	30
Variable O&M cost [$/kWh]	0.001	0.002	0.004	0.002	0	0	0	0
Maximum availability	0.8	0.7	0.9	0.9	0.4	Estimated output profile		0.8
Conversion efficiency	1.00	0.40	0.50	0.37	–	–	–	–

Table 4
Cost assumptions for Japan nodes (JP-H, JP-E, and JP-W).

	Nuclear	Coal	Gas	Oil	Hydro	Wind	PV	Pumped
Initial cost [$/kW]	4000	2400	1150	1900	6000	1700	2500	6000
Fixed O&M cost [$/kW/yr]	104	48	23	39	70	43	31	70
Variable O&M cost [$/kWh]	0.002	0.005	0.006	0.004	0	0	0	0
Maximum availability	0.7	0.75	0.7	0.9	0.4	Estimated output profile		0.8
Conversion efficiency	1.00	0.42	0.50	0.37	–	–	–	–

Table 5
Cost assumptions for Korea (KR).

	Nuclear	Coal	Gas	Oil	Hydro	Wind	PV	Pumped
Initial cost [$/kW]	3300	1500	800	1900	2500	1600	2250	2500
Fixed O&M cost [$/kW/yr]	86	30	16	39	30	40	34	30
Variable O&M cost [$/kWh]	0.002	0.003	0.005	0.004	0	0	0	0
Maximum availability	0.95	0.9	0.9	0.9	0.4	Estimated output profile		0.8
Conversion efficiency	1.00	0.40	0.50	0.37	–	–	–	–

Table 6
Cost assumptions for Russia nodes (RU-FE, RU-SI, and RU-SK).

	Nuclear	Coal	Gas	Oil	Hydro	Wind	PV	Pumped
Initial cost [$/kW]	2800	2200	1000	1200	2500	1500	2000	2500
Fixed O&M cost [$/kW/yr]	73	44	20	24	30	38	30	30
Variable O&M cost [$/kWh]	0.001	0.005	0.005	0.003	0	0	0	0
Maximum availability	0.8	0.7	0.9	0.9	0.4	Estimated output profile		0.8
Conversion efficiency	1.00	0.40	0.50	0.37	–	–	–	–

multiple sources from international organizations, governments, industries as well as research institutes in order to ensure the validity. Specifically, the initial cost data for 2030 are estimated from IEA and individual economy analyses and projections (IEA, 2010, 2014b; METI, 2015; Skoltech, 2015). The future initial cost of fossil fuel-fired plants and wind power remain similar to the current level, while solar PV shows drastic cost reductions.[5] Annual fixed O&M cost [$/kW/yr] are estimated based on EIA (2013), IEA (2014b) and METI (2015). For variable O&M cost (except fuel cost), in Japan we assumed $2/MWh for nuclear, $5/

[5] IEA (2014b) shows the projected initial cost in 2020 and 2035, and, for example, the initial cost of large scale solar PV in China is projected to decrease by approximately 40% by 2035 compared to the 2012 level.

Table 7
Fuel price assumption in 2030.

	Coal [$/t]	Gas [$/MMBtu]	Oil [$/bbl]
China/Gobi	110.5	9.3	121.5
Russia	99.8		
Japan	140.1	14.4	
Korea	137.3	13.5	

MWh for coal-fired, $6/MWh for gas-fired, and $4/MWh for oil-fired (EIA, 2013; METI, 2015). In other regions we adjusted the variable O&M cost using the ratio of initial cost between Japan and each region. The carbon content of each fuel type is derived from EDMC (2014). Assumptions for own-use of electricity at generating plants, ramp-up/down rate, minimum output level and conversion efficiency are taken from IEA (2014a, 2014c) and METI (2015). Data for storage relies mainly on Komiyama et al. (2015).

In considering the maximum availability for nuclear, fossil fuel-fired and hydro generation, we estimated the values using historical capacity and generation data (JEPIC, 2013; EDMC, 2014; KESIS, 2015). We confirmed that the model reproduces results similar to the actual power system (see Appendix A.2). As for wind and PV, hourly output profiles are given exogenously. We estimated those output profiles for GD (the Gobi Desert) as explained in Section 2.3.3. Because of the limited meteorological information available for some economies, the daily output profiles for other areas rely on the following simple assumptions: the output profile for wind is kept flat at all times in all seasons assuming 20% capacity factor, and, for PV, hourly output profiles in each season are estimated from the estimated or observed profiles in Shiraki et al. (2011) and Zhao et al. (2009). Fossil fuel price assumptions in 2030 in Table 7 have been determined from the best available projections (IEA, 2010; Shinoda, 2013; MUFJ, 2013; Morita, 2013; Ling, 2013; KESIS, 2015). We based these estimates on historical CIF prices for energy importing economies, historical FOB prices for exporting economies, and future import price trends from IEA WEO (2013).

2.3.3. Power output of wind and PV in the Gobi Desert area (GD)

2.3.3.1. Estimated wind output. The seasonal profile of the region-wide wind output in GD is estimated by using long-term wind observation data (Elliott et al., 2001). We used a similar estimation approach to Komiyama et al. (2015). Fig. 5 shows a flow chart for this calculation. Elliott et al. (2001) reports average hourly wind speed data in a day in each month at various sites. We selected five observation sites (Sainshand, Mandalgovi, Center Tuvshin Sukh, Tumurbaatar, and Center Manlai Ummu station), and estimated the weighted average wind speed of the Gobi Desert area. Next, we estimated the equivalent wind speed at the hub height of the wind

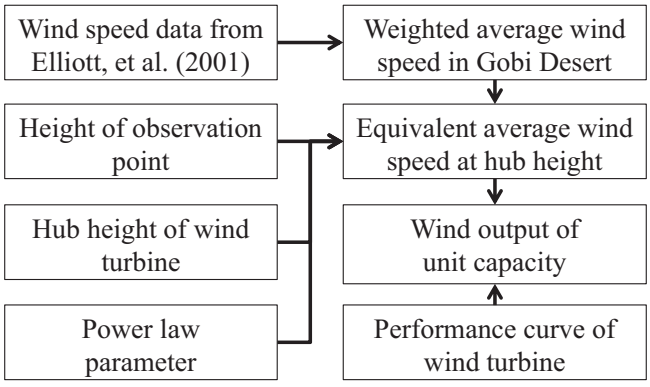

Fig. 5. Flow chart for the calculation of wind power output in the Gobi Desert area.

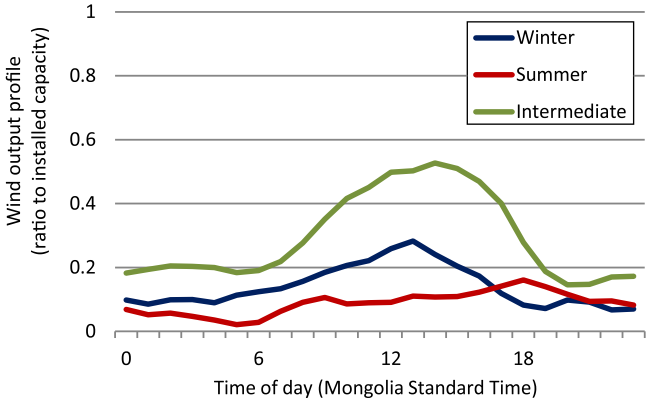

Fig. 6. Assumed daily output profile of wind in the Gobi Desert area (GD).

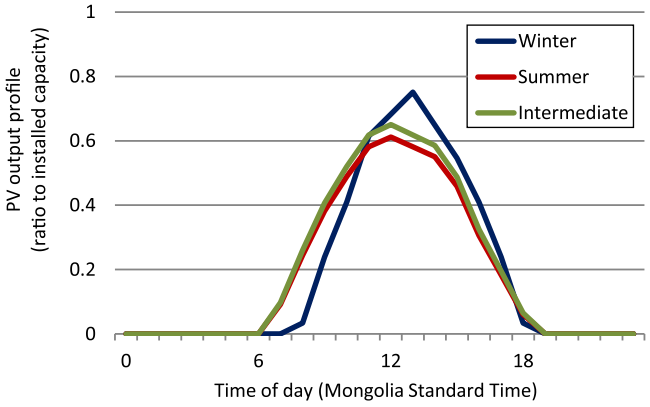

Fig. 7. Assumed daily output profile of PV in the Gobi Desert area (GD).

turbines using the power law, assuming that the measured wind speed is at 10 m and that the *n*-value in the power law is eight. (For discussion of the power law, see Peterson and Hennessey, Jr. (1979).) Then, we calculated the hourly wind turbine output profile (Fig. 6) based on the average hourly wind speed at hub height and a typical power curve.

Wind speed data in January is assumed for the winter season, in July for the summer season. Wind speed in the intermediate season is estimated by averaging the data for April and October. The assumption for the hub height of the wind turbine is 80 m, while the cut-in wind speed, rated speed, and cut-out wind speed are 5 m/s, 12.5 m/s and 25 m/s, respectively. The estimated average wind capacity factor is 26%. The data in Elliott et al. (2001) show the high wind speeds observed in the intermediate season (around April and October) in the Gobi area, and that trend is reflected in Fig. 6.

2.3.3.2. Estimated PV output. We estimated the average solar PV output profile (Fig. 7) by referring to Battushig et al. (2003) and Adiyabat et al. (2006). Battushig et al. (2003) reported the average hourly maximum power of PV modules in October, November, December, March, and April in the Gobi Desert area. PV output profiles depend on various climatic conditions at the sites, such as sunshine duration, air mass and ambient temperature. Because of limited information about detailed solar irradiation in the area, we estimated output profiles by assuming that the observed output shape in April in Battushig et al. (2003) is the representative diurnal variation in the intermediate and the summer season in the Gobi Desert area and that the shape in December represents winter season. We then calculated the PV output profile in each season based on the shapes and the observed daily average PV energy output [Wh/day] in each season in Sainshand city in Mongolia (Adiyabat et al., 2006).

2.3.4. Additional hydro power potential in Russia Far East and Siberia nodes

The assumptions for the additional hydro potential in Russia are based on the estimates by the European Bank for Reconstruction and Development (EBRD) (from IEA (2003)). According to IEA (2003), "economically feasible hydro power capability" in East Siberia and in the Far East is 350 TWh/yr and 294 TWh/yr, respectively. These regions account for 81% of the total potential in Russia. However, hydro resources are widely distributed in the Far East region, which consists of the Far East (or federal) power grid area, the autonomous power grid area and the non-electrified area (IEA, 2003). Similarly, hydro potential in East Siberia is widely distributed from the south border region to the northern part of the region. Only limited parts of the Far East and East Siberia regions have been connected to the federal grid (Popel, 2012). Therefore, we made a simple assumption that one-third of the economical hydro potential of the Far East and Siberia is accessible in practice.

We estimated additional hydro potential on a GW basis using the assumed "accessible potential" (TWh-basis), an assumed capacity factor (40%) and subtracting-off existing capacity (already exploited resources). We equally divided the total additional potential into two categories (Add-Hyd1 and Add-Hyd2) as summarized in Table 8. Initial cost of hydro power potential depends on its geographical location, and in general, undeveloped resources are more expensive than already exploited resources. Thus, this study assumes a higher initial cost for the additional hydro resources compared to already exploited resources. Add-Hyd1 is assumed to be more expensive than the average cost of already exploited resources (Table 6) by 25% and Add-Hyd2 is assumed to be more expensive by 50%.

2.3.5. Transmission lines

HVAC overhead line technology is assumed to be used for overland interconnections, except for the KR∼RU-FE connection, where HVDC technology is proposed in governmental publications (MOTIE, 2014). For undersea connections, HVDC cable technology is assumed. Regarding HVAC substation/switching stations, we assume that one substation/switching station needs to be installed for every 150 km of HVAC overhead transmission line to ensure grid stability. For HVDC connections, we assume AC–DC conversion stations are installed at the each end of the connection. For the connection between JP-E (50 Hz) and JP-W (60 Hz), we assume BTB (Back-to-Back) facilities for frequency conversion.

We estimated transmission line cost by drawing from Bahrman and Johnson (2007), Schaber et al. (2012) and Matsuo et al. (2015). We assume substation/switching station costs of $240M/station and AC–DC conversion station costs of $480M/station, all for stations of 3 GW of capacity. We also assume $1.2M/km for overhead line (rated power: 3 GW) and $7.2M/km for HVDC submarine cable (rated power: 3 GW). Assumed transmission distances are as shown in Fig. 2. The linear programming model requires that interconnection capacity costs be expressed as cost per unit of capacity, so we calculated the initial cost for each transmission route [$/kW] as shown in Table 9. Assumed lifetime, transmission losses and annual fixed O&M cost are 40 years, 5%/1000 km and 0.3% in a ratio to initial cost for all line types, respectively (Bahrman and Johnson, 2007; Matsuo et al., 2015).

Fig. 8 shows the initial capacity assumptions (*LMI* in Eq. (A.11) in Appendix A.1) for transmission lines. We set initial capacity referring to existing capacity and planned additions announced by power utilities or transmission companies (TEPCO, 2014; HEPCO, 2014; SGCC, 2014). No capacity additions are allowed in the *Base* scenario (*LMA*=*LMI*), and we do not constrain capacity additions in the other scenarios ($LMA = \infty$). Instead, the constraint on the net imports to each city node (Eq. (A.26) in Appendix A.1) indirectly regulates the maximum transmission capacity level.

2.3.6. Operating reserve margin

As our study focuses on hourly dispatch, we assumed operating reserve margins in Eq. (A.25) in Appendix A.1 as follows: 10% for China, Japan and Korea and 15% for Russia referring to general criteria and/or historical data (Electric utility course (2008) and

Table 8
Assumptions for additional hydro plants.

	Additional hydro potential [GW]		Initial cost [$/kW]
	RU-FE	RU-SI	
Add-hyd1	12	5	3125
Add-hyd2	12	5	3750

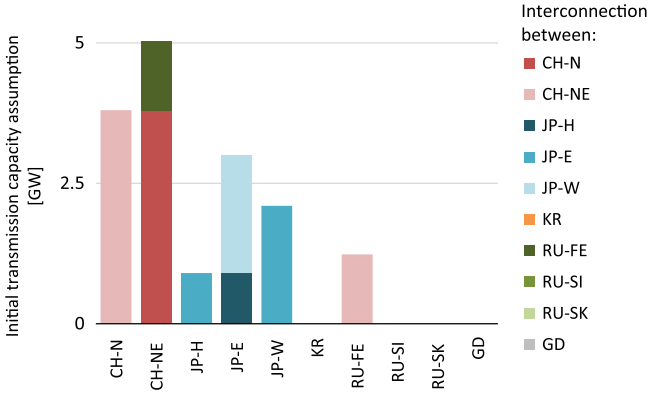

Fig. 8. Initial capacity settings of transmission lines.

Table 9
Initial cost assumptions for each interconnection route [$/kW][a].

	CH-N	CH-NE	JP-H	JP-E	JP-W	KR	RU-FE	RU-SI	RU-SK	GD
CH-N	–	700	–	–	–	1992	–	–	–	840
CH-NE	700	–	–	–	–	–	1360	–	–	1256
JP-H	–	–	–	1392	–	–	–	–	1288	–
JP-E	–	–	1392	–	672	–	–	–	–	–
JP-W	–	–	–	672	–	1840	–	–	–	–
KR	1992	–	–	–	1840	–	1560	–	–	–
RU-FE	–	1360	–	–	–	1560	–	–	1548	2900
RU-SI	–	–	–	–	–	–	–	–	–	1092
RU-SK	–	–	1288	–	–	–	1548	–	–	–
GD	840	1256	–	–	–	–	2900	1092	–	–

[a] "–" Indicates that interconnections are not allowed in this study.

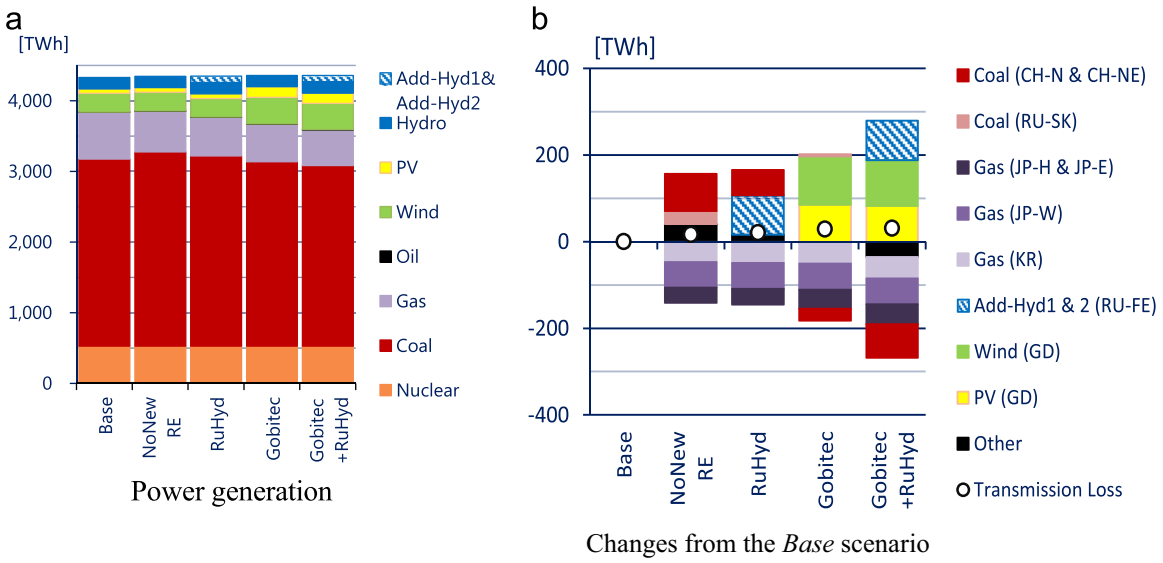

Fig. 9. Power generation in NEA region and changes from the Base scenario.

FEPC (2010) for Japan, KPX (2015) for Korea and SO UPS (2014b) for Russia. As for the China nodes, we assumed a level similar to Japan and Korea, due to limited data availability).

3. Results and discussion

3.1. Power generation mix and capacity

Fig. 9 displays the power generation (NEA total) for each scenario and changes from the Base scenario.

Fig. 9(a) indicates that coal-fired generation remains the dominant source in this region (59–63%) even under the *Gobitec+RuHyd* scenario. In the *Base* scenario, coal-fired electricity accounts for 61% of total generation, and it increases to 63% in the *NoNewRE* scenario. This is because grid interconnection allows high electricity cost regions (like Japan and Korea) to access cheaper coal electricity from China and Russia. The *NoNewRE* scenario in Fig. 9(b) shows coal-fired generation in the China nodes and Russia Sakhalin (RU-SK) replace gas-fired generation in Japan (JP-H, JP-E and JP-W) and Korea (KR). This result implies that cost optimal grid interconnections without expanding renewable energy potentially increases coal-fired generation in China and Russia. This situation might be undesirable especially for China, which is suffering from severe air pollution.

Deployments of renewables in Eastern Russia and the Gobi Desert contribute to an environmentally-friendly generation mix in NEA. Renewables account for 11% of power generation both in the *Base* and the *NoNewRE* scenario, and increase to 13%, 16% and 18% in the last three scenarios, respectively. In the *RuHyd* scenario, additional hydro generation in Eastern Russia, not coal-fired generation in CH-N, mainly replaces gas-fired generation in JP-W and KR (Fig. 9(b)). Yet, China still exports coal-fired generation as Japan and Korea have room for further imports. In the last two scenarios, gas-fired generation in Japan and Korea as well as coal-fired generation in CH-N are replaced by renewable electricity from GD (the Gobi Desert) or Eastern Russia. The gap between the incremental generation and the generation decreases elsewhere represent cross-boundary transmission losses. Our results indicate that 15% and 11% of the transmitted electricity is lost through long distance transmission in the last two scenarios, respectively.

Fig. 10(a)–(e) show the power generation mix and net imports share by region. Electricity trade is very limited in the *Base* scenario. The net imports share is not more than 0.6%. In the *NoNewRE* scenario, the share of net imports increases in Japan Hokkaido (JP-H) and the eastern parts of Japan (JP-E) to 7% and 8.5% of annual demand, respectively. These nodes import mainly from the newly installed fossil fuel-fired coal plants in Sakhalin with a capacity of 5 GW. As noted in Section 2.2, the model limits net transmission inflows to each city node to the reserve margin at all times, reflecting a likely concern over secure electricity supply (see Eq. (A.26) in Appendix A.1). These reserve margins are assumed to be 10% for China, Japan and Korea and 15% for Russia. In JP-W and KR, the net imports almost reaches this upper bound on average. The main exporter to these nodes is China (see also Section 3.3).

In the *RuHyd* scenario, large scale hydro developments in RU-FE allow KR, JP-W and JP-E to import hydroelectricity from Russia instead of fossil fuel-fired electricity from China or Russia. The net imports share in these importing nodes remains similar in level to the *NoNewRE* scenario. In the *Gobitec* scenario, the 'Gobi electricity' increases the net imports in CH-NE to 2%, which results in reducing coal-fired generation in the China nodes. In the *Gobitec+RuHyd* scenario, the annual imports of the two China nodes amount 78 TWh/yr (net imports share: 3% in both nodes). The net imports share almost reaches the upper bound not only in JP-W and KR but also in JP-H and JP-E.

3.2. CO_2 emissions

Fig. 11 displays direct CO_2 emissions in NEA from fossil fuel combustion. Larger coal-fired generation in the *NoNewRE* scenario results in higher emissions by 66Mt-CO_2 (+2.3%) compared to the *Base* scenario. This result implies that interconnection without renewable resource expansion could increase CO_2 emissions in NEA. In the *RuHyd* scenario, additional hydro developments in Eastern Russia slightly reduce the emissions by 0.4 Mt-CO_2 (−0.01%). In the *Gobitec* and *Gobitec+RuHyd* scenarios, Gobi electricity or Gobi electricity+hydro in Eastern Russia contribute to emissions reductions of about 85 Mt-CO_2 (−3.1%) and 148 Mt-CO_2 (−5.3%), respectively. These last two scenarios result in larger reductions as the massive renewable deployments replace carbon-intensive coal-fired electricity in China (see Fig. 9(b)). The limited benefit to emissions in the *RuHyd* scenario is because the emissions from exported coal-fired generation in China (Fig. 9(b)) partly offset the reductions from hydro in Russia.

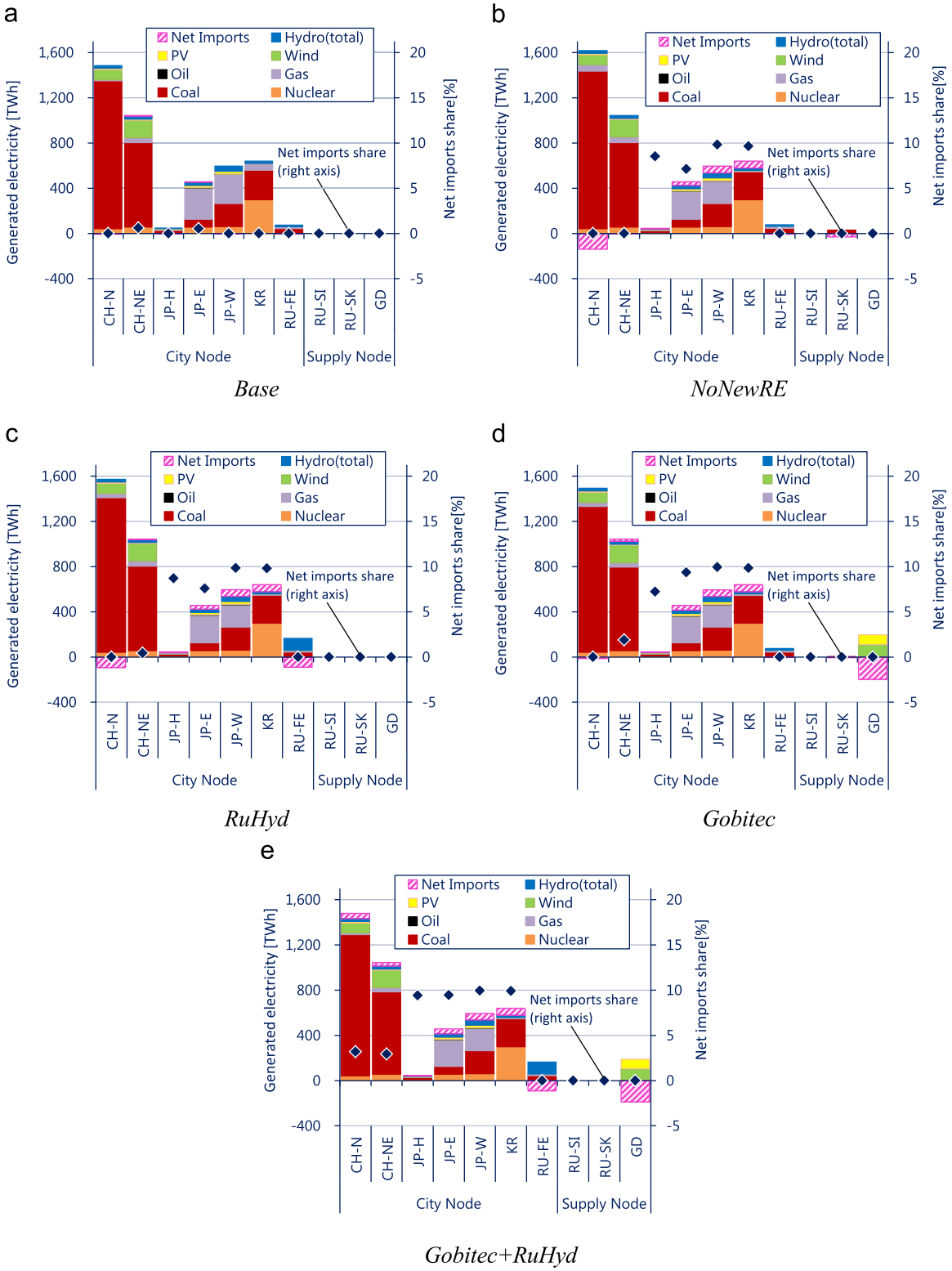

Fig. 10. Power generation mix and net imports by node. Hydro (total) indicates a sum of hydro, additional hydro-1 and additional hydro-2.

The CO_2 reduction in the *Gobitec* scenario that we calculate (85 Mt-CO_2) is lower than that from Energy Charter et al. (2014) (187 Mt-CO_2). (Please note that Energy Charter et al. (2014) mentioned a 187 Gt-CO_2 reduction, but we suspect the units were misstated.) The CO_2 reduction differences are partly because of two factors. First, in Energy Charter et al. (2014), the assumptions for utilization factor for both PV and wind are 30%, which are much higher than our estimates (20% for PV and 26% for wind). Second, the two models use a substantially different dispatch logic for Gobi electricity. Energy Charter et al. (2014) assumed that 80% of Gobi electricity is sent to coal-intensive (high CO_2 emissions per kWh) China, and they use average emissions factors in each importing region to estimate CO_2 emission reductions. On the other hand, our model determines the share of Gobi electricity at each

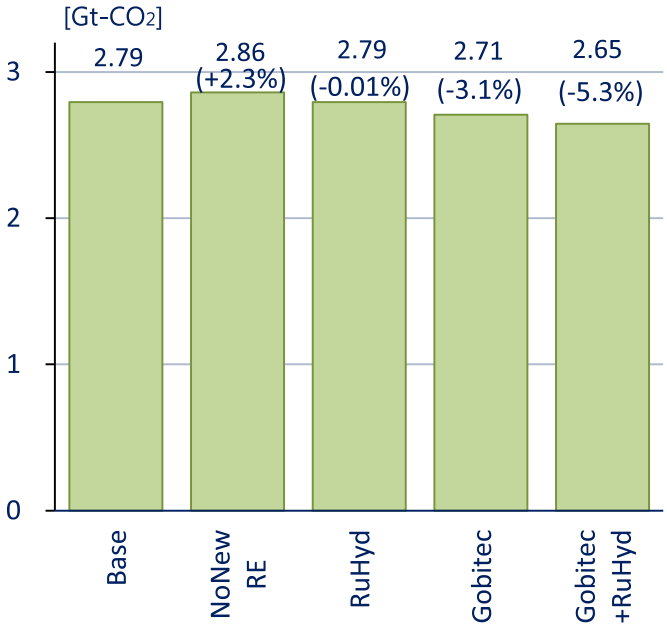

Fig. 11. CO_2 emissions in NEA region.

importing node based on total system cost minimization. Thus, as shown in Fig. 9(b), the increase in Gobi electricity results in reducing high cost gas-fired generation (with relatively low CO_2 emissions per kWh) in Japan and Korea.

3.3. Cross-boundary electricity flow

Fig. 12 indicates cross-boundary electricity flows [TWh/yr] and transmission capacity [GW]. The *Base* scenario shows an international power trade only between Russia Far East (RU-FE) and Northeast China (CH-NE).

In the *NoNewRE* scenario, China and Russia export to Japan and Korea because of low-cost electricity. Korea becomes a net importing economy as well as playing the role of a transit ("bridge") economy between China/Russia and Japan. The economy imports 131 TWh/yr from China, and exports to 66 TWh/yr to Japan. Transmission line capacity of the China–Korea and Korea–Japan interconnections are 21 GW and 11 GW, respectively, which are equivalent to 17% and 9% to the total installed capacity of Korea. The figure also shows the newly added interconnections from Russia Sakhalin to the eastern parts of Japan via Hokkaido (JP-H). By contrast, the transmission capacity from the 'mainland' Russia Far East region (RU-FE) to Japan and Korea is relatively small compared to the aforementioned connections. The limited transmission scale is probably because of the higher transmission cost associated with the longer transmission distances.

On the other hand, in the *RuHyd* scenario, RU-FE becomes a major exporter to Japan and Korea. The majority of the additional hydroelectricity in RU-FE is transmitted to KR (51 TWh/yr). Also, instead of fossil fuel-fired electricity, Russia exports hydroelectricity to Japan (31 TWh/yr), of which 80% are consumed in JP-E rather than JP-H due to the larger scale of the JP-E electricity market. The *Gobitec* scenario shows the large-scale cross-border electricity flow from the Gobi Desert area to Korea and Japan. Transmission lines with a capacity of 100 GW are installed from GD (the Gobi Desert) to match the capacity of the variable renewables there. Yet the utilization rate of these connections, i.e., 22% in the GD–CH-N connection, is relatively low because of the intermittency of the transmitted power. In the *Gobitec+RuHyd* scenario, transmitted electricity from China to Korea decreases compared to the *Gobitec* scenario because Korea imports power from Russia rather than China. Instead, China consumes more of the Gobi Desert electricity, resulting in lower fossil fuel-fired generation in the China nodes.

Electric utilities and transmission companies in Russia, in cooperation with organizations in neighboring economies, have been exploring the possibilities of cross-border grid interconnection (Smirnov, 2012; Inter RAO, 2013). Our results indicate that exporting fossil fuel-fired electricity from Sakhalin to Japan could be an economic option. By contrast, the scale of connections from RU-FE is relatively small in the *NoNewRE* and *Gobitec* scenarios, and it greatly expands under the *RuHyd* and *Gobitec+RuHyd* scenarios in order to export additional hydro power. The results imply that additional hydro power can stimulate opportunities for electricity trade between the 'mainland' Russia Far East and other regions.

3.4. Costs and benefits

Fig. 13 depicts yearly total system cost and its changes from the *Base* scenario. The costs shown include a carbon cost of \$30/t-CO_2 (see Table 1). The total system cost declines by \$2.2B/yr, \$5.0B/yr, \$1.4B/yr, and \$3.4B/yr from *Base* in the *NoNewRE*, *RuHyd*, *Gobitec*, and *Gobitec+RuHyd* scenarios, respectively. These values are equivalent to 0.4–1.3% reductions; therefore, the impacts of interconnection on total system cost appear to be modest. The annualized share of initial cost of cross-boundary transmission to total system cost is relatively small, e.g., 2.1% in the *Gobitec+RuHyd* scenario.

However, grid interconnection affects some components of the total system cost more significantly. As shown in the last three scenarios in Fig. 13(b), while deployment of renewables in Gobi and Eastern Russia and transmission lines have significant initial costs, renewable resource expansion contributes to fuel cost reductions in the NEA region of about 6% (−\$11B/yr), 9% (−\$16B/yr) and 11% (−\$20B/yr) in the last three scenarios, respectively. These results imply two points as follows: first, the benefits of renewable electricity trade mainly depend on fuel cost reductions; second, the main costs which make the power trade and renewable expansion less attractive are the initial costs of renewables and transmission lines.

Large fuel cost savings are estimated in the importing regions, especially in the last scenario: \$3B/yr, \$11B/yr and \$6B/yr in the China nodes, Japan and Korea, respectively, which are equivalent to 5%, 15% and 23% reductions. Nevertheless, these results rely on the future cost assumptions in Section 2.3. In order to investigate the impact of future cost uncertainties on the economics of grid interconnection, we perform a sensitivity analysis on the assumptions for fuel cost and the initial cost of transmission lines and renewable energy in Section 3.6.

Given the time differences among the NEA regions, we were curious whether any of the cost reductions were due to diversification of daily peak loading times. To test this hypothesis, we recalculated the *NoNewRE* scenario with the time difference adjustments turned-off (see Eq. (A.7) in Appendix A.1). The indicated cost reductions from diversification of peak loading times were only \$1.4M/yr, which is insignificant given total cost reductions of \$2.2B/yr in the *NoNewRE* scenario compared to the *Base*. Because of the small time difference (one hour) between the main exporter (China) and importers (Japan and Korea), peak-hours still occur more or less simultaneously in each region, resulting in the modest effects of time differences. This result implies that the benefits of interconnections are mainly due to other factors, such as low-cost electricity in the exporting regions, as well as seasonal load curve variations among the regions.

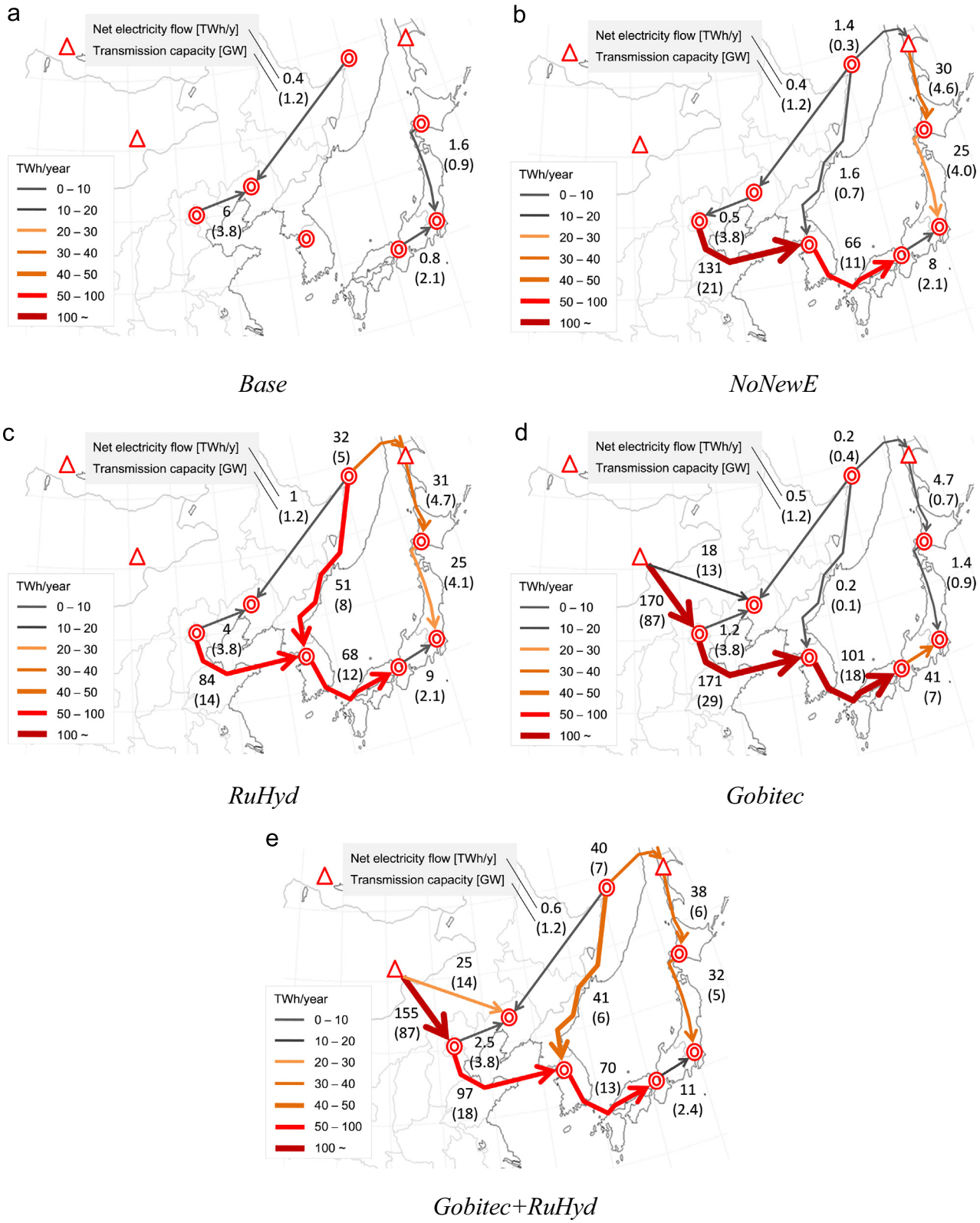

Fig. 12. Annual electricity flow in NEA.

3.5. *Marginal generation costs*

The dual solution to Eq. (A.7) in Appendix A.1 indicates the marginal costs of electricity generation, which are determined by the variable cost of generation, storage, and transmission. The marginal costs are important indicators of the electricity price level (IES, 2004; Schaber et al., 2012). Fig. 14 shows the power generation profile and marginal generation costs in the winter peak season in JP-H in the *Base* and *Gobitec+RuHyd* scenarios as an example. A comparison of the two figures indicates that power imports reduce gas-fired generation and contribute to a lowering of prices, especially during the daytime (around 9:00–11:00 and

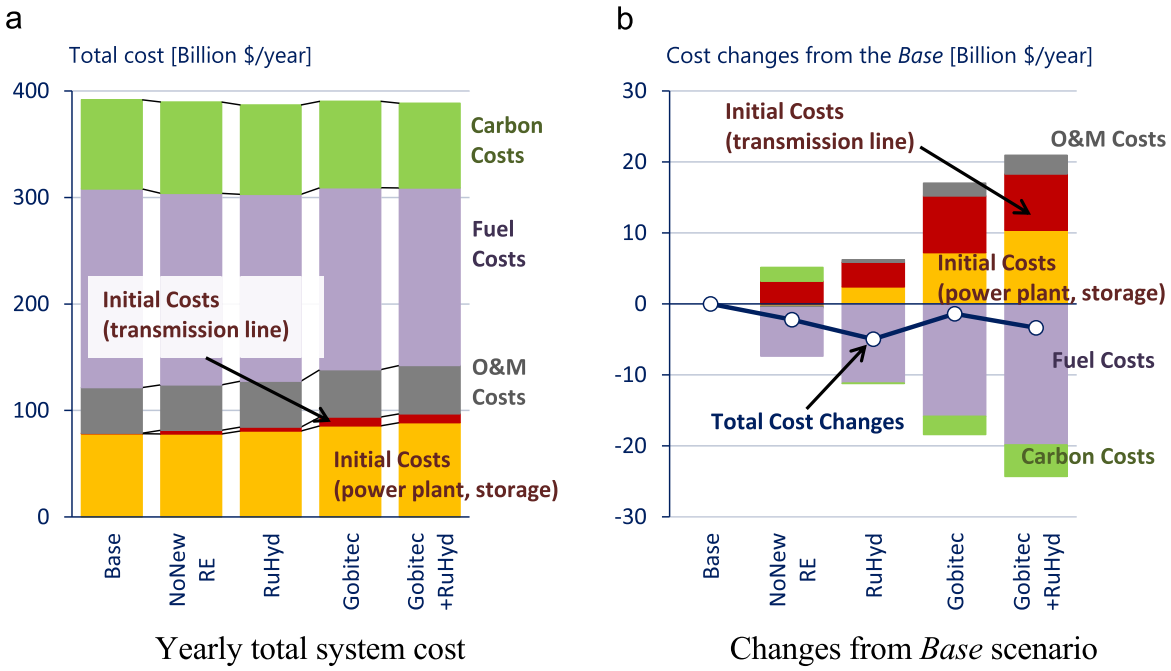

Fig. 13. Yearly total system cost of the NEA region and changes from the Base scenario.

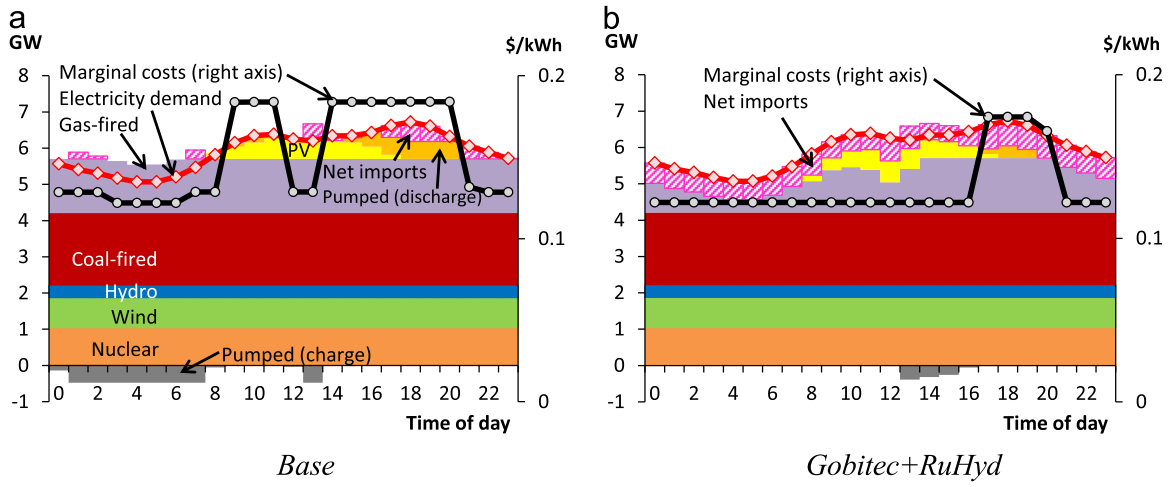

Fig. 14. Power generation profile and marginal generation costs in the winter peak season in the Japan-Hokkaido node (JP-H).

13:00–20:00). For example, at around 14:00, the marginal costs drop from $0.18/kWh in the *Base* scenario to $0.12/kWh in the *Gobitec+RuHyd* scenario.

Fig. 15 presents the average marginal generation costs in the city nodes for the five scenarios. For the China nodes and the Japan nodes (except JP-H), the figure shows weighted average values. The average marginal costs varies from economy to economy in NEA; it ranges from 0.075$/kWh in the China nodes to 0.107$/kWh in Korea and 0.137$/kWh in Japan (except JP-H) in the *Base* scenario. Grid integration lowers the average marginal costs mainly in electricity importing regions. In particular, the Japan Hokkaido area (JP-H) and Korea (KR) show relatively large reductions as the power imports significantly decrease or almost replace high-marginal cost generation, such as oil-fired and gas-fired generation, as shown in Figs. 10 and 14. In the *NoNewRE*, the average marginal costs drops by 0.014$/kWh in JP-H and by 0.003$/kWh in Korea, which are equivalent to 11% and 3% reductions, respectively. As for the last three scenarios, the average marginal costs in Korea remain at a similar level to the *NoNewRE* scenario, while the costs in JP-H decrease in the *Gobitec+RuHyd* scenario due to the increase in power imports (see Fig. 10(d) and (e)).

The Japan nodes, except JP-H, show small changes in average marginal generation costs as the share of high marginal cost generation is relatively large compared to JP-H, and the limited imports (which must be kept less than the reserve margin) are not enough to eliminate them (see Fig. 16). After the nuclear power plant accident in Japan, electric utilities across the economy raised residential electricity prices by 13–37% (from March 2011 to July 2014) primarily because of additional fuel costs (NHK, 2014), and proposals for grid interconnection received increasing attention in Japan as one of the potentially effective measures for lowering prices. Our results indicate that parts of Japan would locally enjoy lowered prices from grid interconnections. Yet, in Japan as a whole, even with the accelerated renewable developments, the price reductions would be relatively small compared to the increases after the nuclear accident, at least as long as imports are constrained due to energy security concerns.

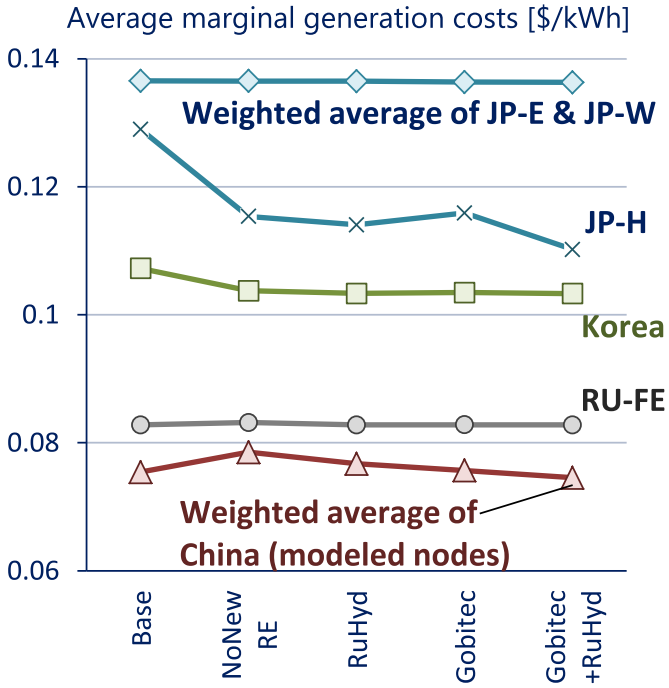

Fig. 15. Average marginal generation costs in the city nodes.

3.6. *Sensitivity analysis of energy prices and initial costs*

Fig. 13 suggested that the benefits achieved by interconnecting power grids and promoting trade in renewable electricity depend mainly on fuel cost savings, and that higher initial cost of renewables and transmission lines makes regional interconnections less attractive. In this section, we conduct a sensitivity analysis on these two factors to investigate their impacts on the economics of grid interconnection. We calculated fifty cases total as shown in Table 10: two installed capacity settings (generation, storage and transmission capacity are fixed to the *Base* or *Gobitec+RuHyd* scenario result) × five fossil fuel prices (−20%, −10%, 0% (="Ref."), +10%, +20% from Table 7) × five initial costs of renewable energy in the Gobi Desert and Russia and all transmission lines (−20%, −10%, 0% (="Ref."), +10%, +20%). Other assumptions are the same as shown in Tables 2–6 (Section 2.3).

Fig. 17 illustrates the economic benefits of the *Gobi+RuHyd* scenario in each case (total system cost reductions compared to *Base*). The results show improved economic viability of grid interconnections under lower initial cost or higher fossil fuel prices. For example, the benefit increases to $12B/yr in the +20% fossil fuel price and −20% initial cost case (this benefit is approximately equivalent to a 3% total cost saving). On the other hand, the results also suggest the benefit would shrink or become negative with 10–20% lower fuel prices and higher initial costs. In Sections 3.1–3.5, we assumed estimated initial costs of renewables and transmission lines in 2030 based on IEA (2014b), Bahrman and Johnson

Table 10
Case settings of sensitivity analysis (50 cases total).

Installed capacity settings of generation, storage and transmission facilities	Fixed to the *Base* or *Gobitec+RuHyd* scenario result
Initial cost changes for renewables (Gobi Desert and Russia) and transmission lines	−20%, −10%, 0% (="Ref."), +10%, +20%
Fossil fuel price changes from Table 7	−20%, −10%, 0% (="Ref."), +10%, +20%

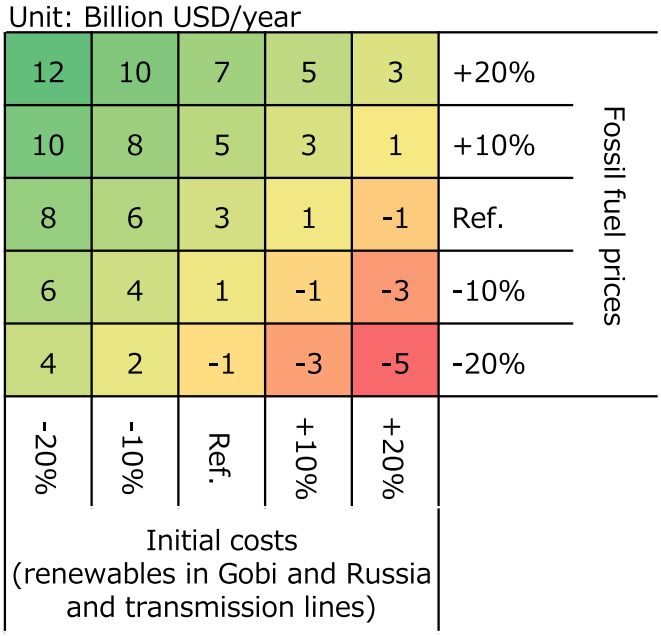

Fig. 17. Economic benefits of the Gobi+RuHyd scenario in each case.

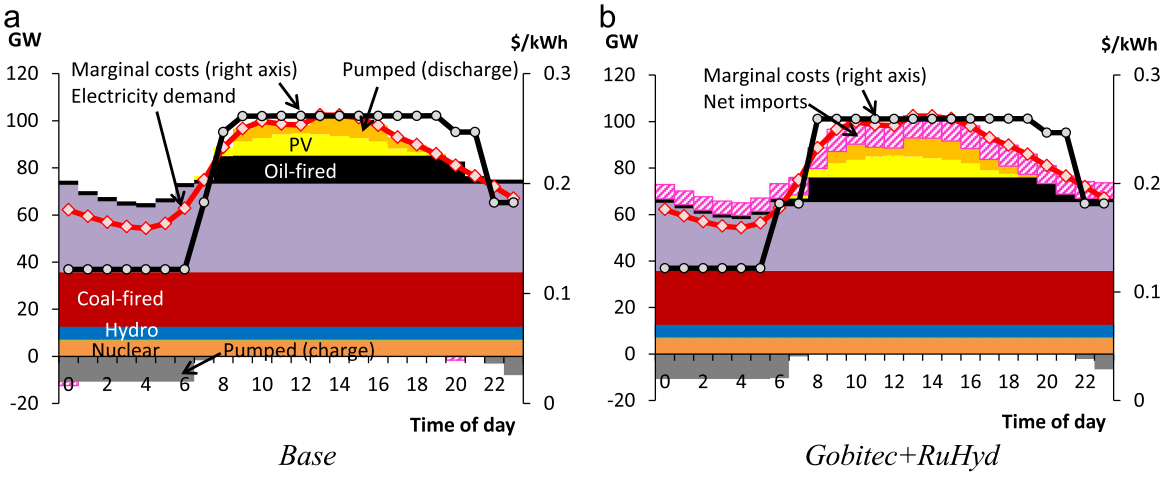

Fig. 16. Power generation profile and marginal generation costs in the summer peak season in Japan West node (JP-W).

(2007) and so on. However, these costs, especially for hydro generation and transmission lines, depend on site-specific characteristics. Also, IEA (2014b) assumes learning rates which reduce the future initial costs of renewables, yet uncertainties exist in these cost reduction trends. Similarly, energy prices have shown their volatile nature in the past decade. The relevant planning organizations should carefully assess the actual initial costs and long-term fossil fuel price trends, bearing in mind their significance, as indicated Fig. 17.

4. Conclusions and policy implications

This study quantitatively investigated the economic viability of power grid interconnections in NEA and renewable energy developments in the Gobi Desert and Eastern Russia with a single-year multi-region power system model. The model is formulated as a linear program, which aims to minimize overall system cost. The model considers nodal electric load characteristics, including representative hourly load curves, as well as the output profile of variable renewables in the Gobi Desert. We validated our model capability using historical data (see Appendix A.2).

We investigated five scenarios for the NEA power system of 2030: *Base*, *NoNewRE*, *RuHyd*, *Gobitec* and *Gobitec+RuHyd* scenarios (see Table 1). Major results in each scenario are summarized in Table 11. These simulation results lead us to several interesting findings as follows.

First, from an environmental perspective, the *Gobitec+RuHyd* scenario shows that access to wind/solar resources in the Gobi Desert and additional hydro resources in Eastern Russia promotes an environmentally-friendly generation mix. The total renewable share in NEA increases from 11% to 18% of which 2% is from Russia and the remaining 5% is from the Gobi Desert. Deployment of these renewables contributes to NEA emission reductions of 5.3%. By contrast, the *NoNewRE* scenario shows that cost-optimal grid interconnections without renewable energy development would promote low-cost coal generation in China and Russia, resulting in an *increase* in CO_2 emissions in NEA (+2.3% from the *Base*) and potentially worse air pollution in China. Thus, interconnection projects should be undertaken in tandem with renewable energy expansion in order to reap both economic and environmental benefits.

Second, all grid interconnection scenarios indicate that economic benefits in the form of total cost reductions depend mainly on the fuel cost saved by shifting to cheaper fossil fuel or to renewables. Expanding renewable energy results in larger fuel cost savings, for example the 4% reductions (−$7B/yr) in the *NoNewRE* versus the 11% reductions (−$20B/yr) in the *Gobitec+RuHyd*. However, the total system cost reductions appear modest (less than 1.3% reduction from the *Base*) due to the increase in initial costs and O&M costs. In addition, sensitivity analysis on fuel price and initial costs (see Section 3.6) imply that the benefit potentially shrinks or becomes negative with 10–20% lower fuel prices and higher initial costs. These limited economic benefits are likely to be a major challenge to implementing grid interconnection in NEA. The relevant planning organizations should carefully assess the actual initial costs and long-term fossil fuel price trends in order to assure that implementation will be beneficial.

Table 11
Summary of the results of each scenario.

	Base	*NoNewRE*	*RuHyd*	*Gobitec*	*Gobitec +RuHyd*
Annual total cost	$392 B/yr	$390B/yr	$387B/yr	$390 B/yr	$388 B/yr
Annual initial costs	$79B/yr	$81B/yr	$84B/yr	$94B/yr	$97B/yr
Annual fuel costs	$187B/yr	$180B/yr	$175B/yr	$171B/yr	$167B/yr
Annual CO_2 emissions (Gt)	2.79 Gt	2.86 Gt	2.79 Gt	2.71 Gt	2.65 Gt
Share of coal-fired generation in NEA (%)	61%	63%	62%	60%	59%
Share of renewables in NEA (%)	11%	11%	13%	16%	18%

Third, the *RuHyd* and *Gobitec+RuHyd* results imply that interconnection opportunities between 'mainland' Russia Far East and the rest of NEA expand with additional hydro development in Eastern Russia. Hence, access to additional hydropower will be the driver of opportunities for grid interconnections between Russia and other regions.

Turning to priorities for future work, Section 3.6 mentioned the importance of site-specific characteristics to the cost of renewables and transmission lines. Further examination of site-specific costs, as well as site-specific performance of renewables, should be undertaken. For example, if detailed meteorological data were available in each node (i.e., hourly or more detailed data for a full year), future work could better characterize the output of intermittent renewables.

Future work should perform sensitivity analysis on the upper bounds for net imports in importing regions and the installed capacity of renewables in the Gobi Desert. Future work might examine alternatives to the transmission route through the DPRK in order to mitigate political risk. And future work might test constraining the output of gas-fired generation in Japan, Korea and China in the alternative cases to *Base* levels, thereby forcing renewables to mainly replace coal-fired generation, for environmental reasons.

Our modeling approach includes some simplifications that should be addressed in future work. The single-year simulation could be replaced with a multi-year simulation in order to examine the evolution of costs and benefits over time. Perhaps most importantly, the current model is deterministic in nature. Incorporating probabilistic representations could improve the robustness of the model in at least two ways. First, incorporating probabilistic behavior into the representation of intermittent renewables would allow a more detailed examination of NEA-wide grid integration issues, not only for the Gobi Desert renewables discussed in this paper, but also for intermittent renewables in the other NEA economies. Second, a probabilistic representation of the performance of additional system components (transmission lines and thermal generating facilities) would allow the model to address the impact of NEA grid interconnection on power system reliability and the costs of maintaining reliability.

Acknowledgment

We would like to sincerely thank Brantley Liddle, formerly Special Advisor at the Asia Pacific Energy Research Centre (APERC), for his guidance and informative comments, as well as four anonymous referees for their helpful suggestions for improvement. The research reported in this paper was generously supported by APERC. The views expressed, however, are those of the authors and not necessarily those of APERC.

Appendix A

A.1. Mathematical formulation

We describe the equations of the model in order to provide a detailed understanding of this study. Table A1 shows the endogenous variables of the model.

Table A1
Endogenous variables in the multi-region power system model.

TC: total annual cost [$/yr]
$xp_{n,p,s,t}$: output of generation type p at local time t in season s in node n [kW]
$de_{n,p,s,t}$: suppressed output of generation type p (p=wind or PV) at local time t in season s in node n [kW]
$mp_{n,p,s}$: daily maximum output of generation type p in season s in node n [kW]
$kp_{n,p}$: capacity of generation type p in node n [kW]
$xl_{n,n2,l,s,t}$: exported power from node n to node $n2$ via line type l at time t (node n time) in season s [kW]
$kl_{n,n2,l}$: total transmission capacity between node n and $n2$ via line type l [kW]
$xch_{n,st,s,t}$: electricity charge of storage type st at local time t in season s in node n [kW]
$xdc_{n,st,s,t}$: electricity discharge of storage type st at local time t in season s in node n [kW]
$ste_{n,st,s,t}$: stored electricity of storage type st at local time t in season s in node n [kWh]
$kst_{n,st}$: kW-capacity of storage type st in node n [kW]

where n, $n2\in$ {1:CH-N, 2:CH-NE, 3:JP-H, 4:JP-E, 5:JP-W, 6:KR, 7:RU-FE, 8:RU-SK, 9:RU-SI, 10:GD}
$s\in$ {1:Summer-Peak, 2:Summer-Average, 3:Winter-Average, 4: Winter-Peak, 5: Intermediate }
$t\in$ {0 , 1, … , 23}
$p\in$ {1:Nuclear, 2:Coal-fired, 3:Gas-fired, 4:Oil-fired, 5:Hydro, 6: Wind, 7:PV, 8: Additional hydro 1 (Add-Hyd1), 9:Additional hydro 2 (Add-Hyd2)}
$st\in$ {Pumped Hydro Storage}
$l\in$ {HV interconnection}

A.1.1. Objective function

Eq. (A.1) is the objective function. This model minimizes total system cost for a single representative year. System cost is composed of annualized initial cost, O&M cost, fuel cost and carbon cost for the whole of Northeast Asia (NEA). The cost of power generation includes all four cost components. The cost of storage and transmission lines consists of initial cost and fixed O&M cost. Therefore, the model chooses cross-boundary power trade if its benefit (usually the savings in generation cost) is larger than the transmission line cost.

Eqs. (A.2)–(A.5) describe each component. In Eq. (A.2), annualized initial cost of generation, storage and transmission facilities are calculated as the product of a capital recovery factor (*PA*, *STA* and *LA*, respectively), unit construction cost and installed capacity. For capital recovery factor calculation, the assumed discount rate is 3% and the lifetime assumptions are as discussed in Sections 2.3.2 and 2.3.5. Eq. (A.3) describes the O&M cost of generation (fixed and variable O&M cost), storage (fixed O&M) and cross-boundary transmission lines (fixed O&M). Eqs. (A.4) and (A.5) respectively describe fuel cost and carbon cost for direct emissions. Time slot length in hours (*HW*) is calculated in Eq. (A.6). Assumed season length (*SW*) in months is in Table A2, and time slice length (*TW*) is 1 h.

$$\min.\ TC = \sum_{n} (CI_n + CO_n + CF_n + CC_n) \tag{A.1}$$

Table A2
Assumed length of seasons.

Season	Assumed length [Months]
Summer-peak	0.2
Summer-average	2.8
Winter-peak	0.2
Winter-average	2.8
Intermediate	6.0

$$CI_n = \sum_{p} PA_p \cdot PI_{n,p} \cdot kp_{n,p} + \sum_{st} STA_{st} \cdot STI_{n,st} \cdot kst_{n,st} + \sum_{n2<n} \sum_{l} LI_l \cdot LI_{n,n2,l} \cdot kl_{n,n2,l} \tag{A.2}$$

$$CO_n = \sum_{p} (POF_{n,p} \cdot kp_{n,p} + \sum_{s} \sum_{t} POV_{n,p} \cdot xp_{n,p,s,t} \cdot HW_{s,t}) + \sum_{st} STOF_{n,st} \cdot kst_{n,st} + \sum_{n2<n} \sum_{l} LOF_l \cdot kl_{n,n2,l} \tag{A.3}$$

$$CF_n = \sum_{p} \sum_{s} \sum_{t} PF_{n,p} \cdot xp_{n,p,s,t} \cdot HW_{s,t} \tag{A.4}$$

$$CC_n = \sum_{p} \sum_{s} \sum_{t} CTAX \cdot Carbon_p \cdot xp_{n,p,s,t} \cdot HW_{s,t} \tag{A.5}$$

$$HW_{s,t} = 8760 \cdot SW_s \cdot TW_t / 12 / 24 \tag{A.6}$$

where CI_n: annualized initial cost of generation, storage and transmission facilities in node n [$/yr]; CO_n: annual O&M cost of generation, storage and transmission facilities in node n [$/yr]; CF_n: annual fuel cost in node n [$/yr]; CC_n: annual carbon cost for fuel combustion [$/yr]; PA_p: capital recovery factor for generation type p; $PI_{n,p}$: initial cost for generation type p in node n [$/kW]; STA_{st}: capital recovery factor for storage type st; $STI_{n,st}$: initial cost for storage type st in node n [$/kW]; LA_l: capital recovery factor for transmission lines; $LI_{n,n2,l}$: initial cost of a transmission line between nodes n and $n2$ [$/kW]; $POF_{n,p}$: fixed O&M cost for generation type p [$/kW/yr]; $POV_{n,p}$: variable O&M cost for generation type p [$/kWh]; $STOF_{n,st}$: fixed O&M cost for storage type st [$/kW/yr]; LOF_l: fixed O&M cost for a transmission line [$/kW/yr]; $PF_{n,p}$: fuel cost for generation type p [$/kWh]; $Carbon_p$: carbon intensity for generation type p [t-CO_2/kWh]; *CTAX*: carbon price [$/t-$CO_2$]; $HW_{s,t}$: length of time slot at local time t in season s [h]; SW_s: length of season s [Months] (see Table A2); TW_t: length of time slice t [h] (=1 h).

A.1.2. Constraints and equations

A.1.2.1. Power demand and supply balance

Eq. (A.7) ensures that electricity demand must be satisfied at all times in all seasons and in all nodes. The left part indicates the sum of power supply from domestic generators, net power imports and net power discharge of storage facilities. Cross-boundary transmission losses are considered when transmitted power reaches the importing node by multiplying exported power by transmission efficiency (*xl*LE*). Time differences between power exporting and importing nodes are considered for imported power. *ImT* indicates the local time at the origin of electricity imports defined as below. Note that we number hours of the day from 0 to 23 (Table A1).

The dual solution to this equation indicates the marginal costs of electricity generation. The marginal costs are determined by the variable cost of generation, storage, and transmission. Losses in transmission and storage indirectly increase marginal costs and total system cost, as they lead to higher demand for power generation (Schaber et al., 2012). Eq. (A.8) shows how we calculate cross-boundary transmission efficiency.

This model does not explicitly consider modes of operation of generation and storage facilities. In the real world, storage facilities are either in charging mode (pumping mode for pumped hydro storage), discharging mode (generation mode) or standby mode at any given time. In our linear programming model, Eq. (A.7) technically allows both charging and discharging simultaneously. However, because of the power losses this would involve, as

represented in Eqs. (A.23) and (A.24) below, the model will avoid a solution with simultaneous charging and discharging.

$$\sum_{p} xp_{n,p,s,t} + \sum_{n2}\sum_{l} (xl_{n2,n,l,s,ImT_{n2,n,t}} \cdot LE_{n,n2,l} - xl_{n,n2,l,s,t}) + \sum_{st} (xdc_{n,st,s,t} - xch_{n,st,s,t}) = ELD_{n,s,t} \quad (A.7)$$

$$LE_{n,n2,l} = (1 - LOS_l)^{\frac{DIS_{n,n2}}{1000}} \quad (A.8)$$

where $ELD_{n,s,t}$: electric load at local time t in season s in node n [kW]; $LE_{n,n2,l}$: cross-boundary transmission efficiency for line type l between nodes n and $n2$; LOS_l: transmission loss rate for line type l [per thousand km]; $DIS_{n,n2}$: transmission distance between nodes n and $n2$ [km]; $ImT_{n2,n,t}$: local time at the origin of electricity imports, defined as:

$t + TimD_{n2,n} + 24$ for $t + TimD_{n2,n} < 0$;

$t + TimD_{n2,n}$ for $0 \le t + TimD_{n2,n} < 24$;

$t + TimD_{n2,n} - 24$ for $t + TimD_{n2,n} \ge 24$;

and $TimD_{n2,n}$: time difference between nodes (e.g., $TimD_{CH\text{-}N,KR} = -1$)).

A.1.2.2. Installable capacity constraint

Installable capacity of each technology is constrained by its minimum and maximum deployable limits (see Sections 2.3.2 and 2.3.5 for initial capacity and upper limit assumptions).

$$PMI_{n,p} \le kp_{n,p} \le PMA_{n,p} \quad (A.9)$$

$$SMI_{n,st} \le kst_{n,st} \le SMA_{n,st} \quad (A.10)$$

$$LMI_{n,n2,l} \le kl_{n,n2,l} \le LMA_{n,n2,l} \quad (A.11)$$

where $PMI_{n,p}$: initial capacity for generation type p in node n [kW]; $PMA_{n,p}$: capacity upper limit for generation type p in node n [kW]; $SMI_{n,st}$: initial capacity for storage type st in node n [kW]; $SMA_{n,st}$: capacity upper limit for storage type st in node n [kW]; $LMI_{n,n2,l}$: initial capacity for transmission line type l between node n and $n2$ [kW]; $LMA_{n,n2,l}$: capacity upper limit for transmission line type l between node n and $n2$ [kW].

A.1.2.3. Output constraint

Eqs. (A.12)–(A.16) constrain output of generation, storage and transmission facilities. The output of power generation technologies, except wind power and PV, are constrained to their available capacity (Eq. (A.12)). For wind and PV, the seasonal hourly availability profiles (ROF) are exogenously given in Eq. (A.13). These profiles for Gobi Desert (GD) are estimated in Section 2.3 based on observation data (Elliott et al., 2001). The left part of Eq. (A.13) indicates two destinations for output power from wind and PV: power supplied to the grid (xp) or suppressed (de). Eq. (A.14) constrains the charge to or discharge from storage facilities to their available power capacity (kW-capacity). Eq. (A.15) constrains stored electricity to the energy capacity (kWh-capacity) of the facility, i.e., reservoir capacity for pumped hydro.

$$xp_{n,p,s,t} \le PAV_p \cdot kp_{n,p} (p = 1, \ldots, 5, 8, 9) \quad (A.12)$$

$$xp_{n,p,s,t} + de_{n,p,s,t} = ROF_{n,p,s,t} \cdot kp_{n,p} (p = 6, 7) \quad (A.13)$$

$$xch_{n,st,s,t} + xdc_{n,st,s,t} \le STAV_{st} \cdot kst_{n,st} \quad (A.14)$$

$$ste_{n,st,s,t} \le STAV_{st} \cdot CRT_{st} \cdot kst_{n,st} \quad (A.15)$$

$$xl_{n2,n,l,s,t} + xl_{n,n2,l,s,t} \le LAV_l \cdot kl_{n,n2,l} \quad (A.16)$$

where PAV_p: availability factor for generation type p (p=1, …,5,8,9); $ROF_{n,p,s,t}$: output profile of intermittent renewable (wind and PV) energy at local time t in season s, in node n (p=6, 7); $STAV_{st}$: availability factor for storage type st; CRT_{st}: maximum ratio of kWh to kW for storage type st; LAV_l: availability factor for transmission line type l.

A.1.2.4. Ramping constraint for thermal generation (nuclear and fossil fuel-fired)

The model considers technology-specific ramping constraints for nuclear and fossil fuel-fired plants. For technical reasons, each technology has its own controllability, with output of these generators changeable within their ramping capabilities. Ramping up and ramping down limits are modeled as follows in this study:

$$xp_{n,p,s,t} \le xp_{n,p,s,t-1} + LFR_p \cdot kp_{n,p} (t \ne 0) \quad (A.17)$$

$$xp_{n,p,s,0} \le xp_{n,p,s,23} + LFR_p \cdot kp_{n,p} \quad (A.18)$$

$$xp_{n,p,s,t} \ge xp_{n,p,s,t-1} - LFR_p \cdot kp_{n,p} (t \ne 0) \quad (A.19)$$

$$xp_{n,p,s,0} \ge xp_{n,p,s,23} - LFR_p \cdot kp_{n,p} \quad (A.20)$$

where LFR_p: maximum load following rate for generation type p [/h].

A.1.2.5. Daily minimum output constraint for thermal plants

Eq. (A.21) requires that thermal plants generate electricity at no less than their minimum output threshold. The model calculates the minimum output threshold by multiplying minimum output rate (MOL) and daily maximum output (mp) as described in Eq. (A.21). Daily maximum output for each plant type in each season is determined by Eq. (A.22).

$$xp_{n,p,s,t} \ge mp_{n,p,s} \cdot MOL_p \quad (A.21)$$

$$mp_{n,p,s} \ge xp_{n,p,s,t} \quad (A.22)$$

where MOL_p: minimum output rate of operation for generation type p.

A.1.2.6. Stored energy balance

Eqs. (A.23) and (A.24) relates power charge (xch), power discharge (xdc) and the level of stored electricity (ste). Self-discharge loss and charge/discharge efficiency are considered in this equation.

$$ste_{n,st,s,t} = (1 - SDR_{st}) \cdot ste_{n,st,s,t-1} + \left(\sqrt{CEF_{st}} \cdot xch_{n,st,s,t} - xdc_{n,st,s,t} / \sqrt{CEF_{st}}\right) \cdot TW_t (t \ne 0) \quad (A.23)$$

$$ste_{n,st,s,0} = (1 - SDR_{st}) \cdot ste_{n,st,s,23} + (\sqrt{CEF_{st}} \cdot xch_{n,st,s,0} - xdc_{n,st,s,0} / \sqrt{CEF_{st}}) \cdot TW_t \quad (A.24)$$

where SDR_{st}: self-discharge rate for storage type st; CEF_{st}: cycle efficiency for storage type st; and TW_t: length of time slice t [h] (=1 h).

A.1.2.7. Capacity reserve margin constraint

Constraint (A.25) ensures a certain level of capacity reserve margin in each node in order to maintain a secure and reliable power supply system. There should be enough excess generation and storage capacity at each node to cover demand plus the reserve margin.

$$\sum_{p} kp_{n,p} \cdot PCC_{p} + \sum_{st} kst_{n,st} \cdot STCC_{st} \geq (1 + RVM_{n}) \cdot ELD_{n,s,t} \quad \text{(A.25)}$$

where RVM_n: operating reserve margin in node n; PCC_p: capacity credit for generation type p; $STCC_{st}$: capacity credit for storage type st.

A.1.2.8. Upper constraints on net transmission inflows for city nodes

In general, each power service area needs to be prepared for transmission interruptions. Thus, in the scenarios in this study, the net transmission inflows at each city node (left part of the equation) are limited to be less than the reserve margin level ($NIS = RVM$).

$$\sum_{l,\, n2} (xl_{n2,n,l,s,t} \cdot LE_{n,n2,l} - xl_{n,n2,l,s,t}) \leq NIS_{n} \cdot ELD_{n,s,t} \quad (\text{for } n = 1, \ldots, 7) \quad \text{(A.26)}$$

where NIS_n: maximum share of net transmission inflows in node n (we assume this is equal to the operating reserve margin for the scenarios in this study).

A.1.2.9. Additional hydro power export constraints

As explained in the *RuHyd* scenario in Section 2.2, this study considers additional hydro developments in Russia Far East (RU-FE) and Russia Siberia (RU-SI) for exporting to foreign nodes. This equation ensures that power exports from these nodes should be greater than or equal to the output power of additional hydro (AddHyd-1 and AddHyd-2).

$$\sum_{l,n2 \notin EN_{n}} xl_{n,n2,l,s,t} \geq \sum_{p=8}^{9} xp_{n,p,s,t} \quad \text{(A.27)}$$

A.1.2.10. Transmission line capacity constraints for supply nodes

Eq. (A.28) requires each supply node (GD, RU-SI, and RU-FE) to have enough transmission capacity to deliver the output of the installed generation capacity in the node. This constraint may be active especially in the *Gobitec* and *Gobitec+RuHyd* scenarios, where there are minimum constraints on generation capacity in the Gobi Desert (GD) node. This constraint forces the total GD transmission capacity to at least match the total GD generation capacity.

$$\sum_{l,n2} kl_{n,n2,l} \geq \sum_{p} kp_{n,p} \ (\text{for } n = 8,\ 9,\ 10) \quad \text{(A.28)}$$

A.2. Model validation

In order to validate the model's ability to properly assess the real-world power system, we performed a simulation of the NEA power system for the year 2010, the most recent year before the Great East Japan Earthquake. The installed capacity of generation, storage and cross-boundary transmission facilities is calibrated to historical data (JEPIC, 2012). Costs and fuel prices for 2010 are based on IEA (2010), IEA (2014b) and Energy and Environment Council (2011). Historical average efficiencies of fossil fuel-fired plants are estimated using IEA (2014c). We adjusted the reserve margin for Japan and Korea in 2010 based on available historical data (TEPCO, 2013; MKE, 2013). No carbon tax is assumed and other parameters are the same as shown in Tables 2–6 (Section 2.3).

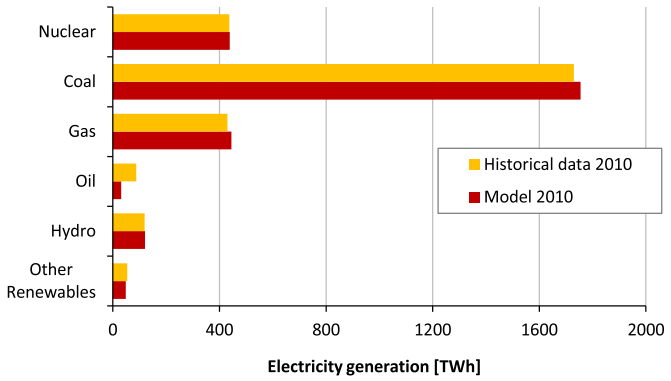

Fig. A1. Comparison of modeled generated electricity and historical data in Northeast Asia.

Fig. A1 compares modeled electricity generation and historical data (JEPIC, 2014). So-called base load and middle load plants (nuclear, coal, gas and hydro) show relatively good fit. By contrast, the model tends to underestimate generation from peak load plants (oil). As reported in Schaber et al. (2012), this is probably because of the deterministic nature of the optimization model. Probabilistic aspects, such as unforeseen forecast errors or generation outages, are not considered in the model, yet peak load plants are often operated to balance electricity demand and supply in those events.

The model reproduces similar trends of cross-boundary electricity trade as shown in Fig. A2. The observed differences might be because the actual power trade is not always scheduled based on cost-optimization, as well as because the model simplifies several aspects of the real world, especially in terms of simplified modeling of electricity flow (see paragraph 7 in Section 2.1) and temporal resolution.

Fig. A3 compares historical average retail electricity prices with modeled average marginal costs of power generation. Unfortunately, we know of no source of historical data on marginal generation costs for the NEA economies. Historical average retail electricity prices were obtained from JEPIC (2012) for China, METI (2014) for Japan, KESIS (2015) for Korea and RAO Energy System of East (2013) for the Russia Far East area. The computed marginal generating costs tend to be lower than the historical retail prices (i.e. 4 c/kWh in Japan and 1 c/kWh in Russia Far East). This is partly because of the additional costs, taxes or subsidies not explicitly

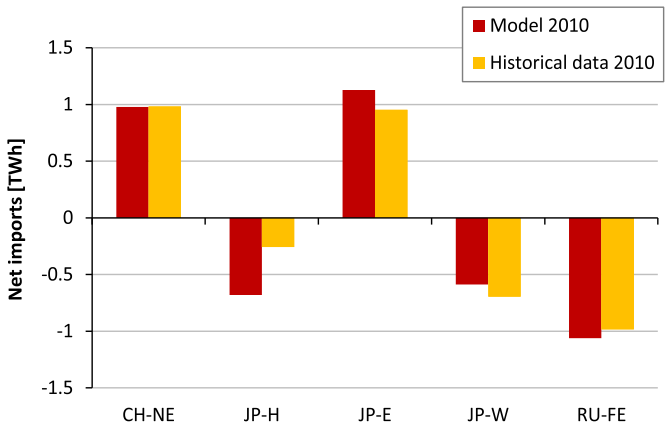

Fig. A2. Modeled net imports and historical data .

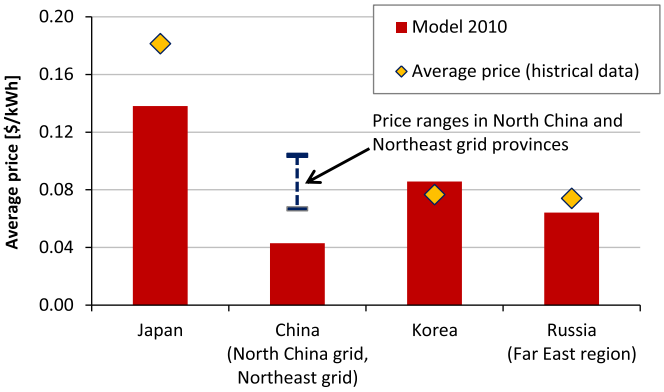

Fig. A3. Comparison of the average retail electricity prices with the modeled average marginal costs of power generation .

included in our model. The historical retail electricity price in Korea is lower than the computed average marginal costs. This is probably because Korea government regulation holds electricity price at a level lower than the actual generating costs. In fact, from 2008 to 2012, Korea Electric Power Corporation was in a chronic state of deficit (KEPCO, 2015).

The generated electricity and cross-boundary trades in the benchmark results are insensitive to fuel price changes: a considerable price increase (90% for coal and 20% for gas) does not have major impacts on the results.

References

Adiyabat, A., et al., 2006. Evaluation of solar energy potential and PV module performance in the Gobi Desert of Mongolia. Prog. Photovolt.: Res. Appl. 14, 553–566.

APERC, 2013. APEC Energy Demand and Supply Outlook, 5th edition. Asia Pacific Energy Research Centre (APERC), Tokyo.

Bahrman, M., Johnson, B., 2007. The ABCs of HVDC transmission technologies. IEEE Power Energy Mag. 5 (2).

Battushig, M., et al., 2003. Performance monitoring of PV modules for VLS-PV systems in Gobi Desert of Mongolia. In: Proceedings of 3rd World Conference on Photovoltaic Energy Convension, May 11–18, 2003, Osaka, Japan.

Bowen, B.H., Sparrow, F., Yu, Z., 1999. Modeling electricity trade policy for the tweleve nations of the Southern African Power Pool (SAPP). Util. Policy 8, 183–197.

Chang, Y., Li, Y., 2013. Power generation and cross-border grid planning for the integrated ASEAN electricity market: a dynamic linear programming model. Energy Strategy Rev. 2, 153–160.

Choi, J., et al., 2006. Probablistic reliability based tie line capacity for interconnecting power systems of South Korea, North Korea and Far East Russia. In: Proceedings of 9th International Conference on Probabilistic Methods Applied to Power Systems, KTH, Sweden, June 11–15.

Chung, K.-H., Kim, B.H., 2007. Economic feasibility on the interconnected electric power systems in North-East Asia. J. Electr. Eng. Technol. 2 (4), 452–460.

EDMC, 2014. Handbook of Energy & Economic Statistics. The Energy Conservation Center, Tokyo, Japan.

EIA, 2013. Updated Capital Cost Estimates for Utility Scale Electricity GEnerating Plants. Energy Information Administration (US DOE), Washington.

Electric utility course, 2008. Electric Power Industry Encyclopedia. Energy Forum, Tokyo (in Japanese).

Elliott, D., et al., 2001. Wind Energy Resource Atlas of Mongolia. NREL/TP-500-28972. Colorado.

Energy and Environment Council, 2011. Report of cost validation committee. Energy and Environment Council (Prime Minister's Office, Japan), Tokyo (in Japanese).

Energy Charter, et al., 2014. Gobitec and Asian Super Grid for Renewable Energies in Northeast Asia. Energy Charter Secretariat.

Eurus Energy, 2012. Solar Power – Requirements. [Online] Available at: ⟨http://eurus-energy.com/en/solar_power/condition.html⟩ (accessed 03.08.15).

FEPC, 2010. Statistics of 60-year Power Industry History in Japan. [Online] Available at: ⟨http://www.fepc.or.jp/library/data/60tokei/⟩ (accessed 27.11.14) (in Japanese).

Google, 2015. Google Map. [Online] Available at: ⟨https://www.google.co.jp/⟩ (accessed 18.08.15).

Government of Japan, 2014. Portal Site about Energy Saving. [Online] Available at: ⟨http://setsuden.go.jp/⟩ (accessed 13.03.15) (in Japanese).

Graaf, T.V. d, Sovacool, B.K., 2014. Thinking big: politics, progress and security in the management of Asian and European energy megaprojects. Energy Policy 74, 16–27.

HEPCO, 2014. Press Release: Started Construction of Additional Transmission Line Between Hokkaido and Honshu-island. [Online] Available at: ⟨http://www.hepco.co.jp/info/2014/1189511_1635.html⟩ (accessed 30.06.15) (in Japanese).

Hippel, D. v., 2001. Estimated Costs and Benefits of Power Grid Interconnections in Northeast Asia. Prepared for the Northeast Asia Grid Interconnection Workshop, Beijing, China, May 14–16, 2001.

Hippel, D. v, Gulidov, R., Kalashnikov, V., Hayes, P., 2011. Northeast Asia regional energy infrastructure proposals. Energy Policy 39, 6855–6866.

IEA, 2003. Renewables in Russia From Opportunity to Reality. International Energy Agency, Paris.

IEA, 2010. Projected Cost of Generating Electricity, 2010 Edition International Energy Agency, Paris.

IEA, 2013. World Energy Outlook 2013. International Energy Agency, Paris.

IEA, 2014a. The Power of Transformation – Wind, Sun and The Economics of Flexible Power Systems. International Energy Agency, Paris.

IEA, 2014b. World Energy Outlook Investment Costs. [Online] Available at: ⟨http://www.worldenergyoutlook.org/weomodel/investmentcosts/⟩ (accessed 13.03.15).

IEA, 2014c. World Energy Statistics, Retrieved from OECD/IEA CD-ROM service.

IES, 2004. The Long Run Marginal Cost of Electricity Generation in New South Wales. Intelligent Energy Systems, Sydney.

Inter RAO, 2013. Bridge of Strategic Importance. Energy Without Borders 4, 16–17.

JAIF, 2013. Electricity situation in Russia. [Online] Available at: ⟨http://www.jaif.or.jp/ja/news/2013/russia_nuclear_development.pdf⟩ (accessed 13.03.15) (in Japanese).

JAIF, 2014. Nuclear Development in China. [Online] Available at: ⟨http://www.jaif.or.jp/ja/asia/china/china_data.pdf⟩ (accessed 13.03.15) (in Japanese).

JEPIC, 2006. Overseas Electric Power Industry Statistics 2006. Japan Electric Power Information Center Inc., Tokyo (in Japanese).

JEPIC, 2012. Overseas Electric Power Industry Statistics 2012. Japan Electric Power Information Center Inc., Tokyo (in Japanese).

JEPIC, 2013. Overseas Electric Power Industry Statistics 2013. Japan Electric Power Information Center Inc., Tokyo (in Japanese).

JEPIC, 2014. Overseas Electric Power Industry Statistics 2014. Japan Electric Power Information Center Inc., Tokyo (in Japanese).

KEPCO, 2014. KEPCO's future plans of Northeast Asia supergrid. Presentation material at "Roadmap to Asian Super Grid", January 2014.

KEPCO, 2015. KEPCO-Comprehensive Income. [Online] Available at: ⟨http://home.kepco.co.kr/kepco/EN/C/htmlView/ENCBHP00501.do?menuCd=EN030206⟩ (accessed 30.06.15).

KESIS, 2015. Korea Energy Statistics Information System. [Online] Available at: ⟨http://www.kesis.net/⟩ (accessed 13.03.15).

KESIS, 2015. Korea Energy Statistics Information System. [Online] Available at: ⟨http://www.kesis.net/flexapp/KesisFlexApp.jsp?menuId=Q0109&reportId=&chk=Y⟩ (accessed 01.01.15).

Komiyama, R., Fujii, Y., 2014. Assessment of massive integration of photovoltaic system considering rechargeable battery in Japan with high time-resolution optimal power generation mix model. Energy Policy 66, 73–89.

Komiyama, R., Otsuki, T., Fujii, Y., 2015. Energy modeling and analysis for optimal grid integration of large-scale variable renewables using hydrogen storage in Japan. Energy 87, 537–555.

KPX, 2015. Acutal value of peak load over past 5 years. [Online] Available at: ⟨http://power.kpx.or.kr/powerinfo_en.php⟩ (accessed 04.08.15).

Kunstýř, J., Mano, S., 2013. Energy Security and Cross-Border Electricity Trade: Can the Asian Super Grid project pose security risks for Japan? Can the electricity imports be used as an extortion weapon? [Online] Available at: ⟨http://jref.or.jp/images/pdf/20140130/Energy_weapon_final.pdf⟩ (accessed 18.02.15).

Lee, S.-S., Park, J.-K., Moon, S.-I., Yoon, Y.-T., 2005. Seasonal load patterns and power flow analysis for interconnection in Northeast Asia. In: IEEE Power Engineering Society General Meeting.

Lilliestam, J., Ellenbeck, S., 2011. Energy security and renewable electricity trade – Will Desertec make Europe vulnerable to the "energy weapon"? Energy Policy 39, 3380–3391.

Ling, S.Y., 2013. China gas price deregulating the market. Platts insight October.

Mano, S., 2014. Asia Super Grid Opportunities and Risks. [Online] Available at: ⟨http://jref.or.jp/images/pdf/20140128/JREF_Roadmap_to_ASG_Session1_Mano.pdf⟩ (accessed 10.07.15).

Matsuo, Y., et al., 2015. Quantitative Analysis of Effects of International Power Grid Interconnection in ASEAN Region. [Online] Available at: ⟨https://eneken.ieej.or.jp/data/5909.pdf⟩ (accessed 30.06.15).

McElroy, M.B., Lu, X., Nielsen, C.P., Wang, Y., 2009. Potential for wind-generated electricity in China. Science 325 (5946), 1378–1380.

METI, 2014. Energy White Paper 2014. [Online] Available at: ⟨http://www.enecho.meti.go.jp/about/whitepaper/2014html/⟩ (accessed 21.01.15).

METI, 2015. Report of Power Generating Costs Working Group. [Online] Available at: ⟨http://www.enecho.meti.go.jp/committee/council/basic_policy_subcommittee/mitoshi/cost_wg/pdf/cost_wg_03.pdf⟩ (accessed 30.05.15).

MKE, 2013. The 6th Basic Plan for Long-term Electricity Supply and Demand [2013–2027]. Ministry of Knowledge Economy, Korea.

Morita, K., 2013. IEEJ Coal Trend No. 10. [Online] Available at: ⟨https://eneken.ieej.or.jp/data/4939.pdf⟩ (accessed 13.03.15).

MOTIE, 2014. Korea Energy Master Plan Outlook and Policies to 2035. Ministry of Trade, Industry and Energy, Korea.

MUFJ, 2013. Coal Market Situation and Outlook in China. [Online] Available at: ⟨https://reports.btmuc.com/fileroot_sh/FILE/information/130313_01.pdf⟩

(accessed 13.03.15).
Nagayama, H., 2014. An analysis of management efficiency at Japanese and Korean electric companies and the effects of business integration. Dev. Eng. 20, 1–15.
NHK, 2014. "Re-raise" the Electricity Price and its Wide Impacts. [Online] Available at: ⟨http://www.nhk.or.jp/ohayou/marugoto/2014/09/0916.html⟩ (accessed 15.02.15).
Peterson, E.W., Hennessey Jr, J.P., 1979. On the use of power laws for estimates of wind power potential. J. Appl. Meteol. 17, 390–394.
Podkovalnikov, S., 2002. Study for Russia, Democratic People Republic of Korea, Republic of Korea and China Power Interconnection: Analysis of Current Status. Energy Systems Institute, Siberian Branch, Russian Academy of Sciences.
Popel, O., 2012. The state and problems of renewable energy development in the world and in Russia. Yaroslavl, Russian tytle: "СОСТОЯНИЕ И ПРОБЛЕМЫ РАЗВИТИЯ ВОЗОБНОВЛЯЕМОЙ ЭНЕРГЕТИКИ В МИРЕ И В РОССИИ" (in Russian).
RAO Energy System of East, 2013. Annual Report 2013: Description of Tariff Policy, Changes in 2013. [Online] Available at: ⟨http://raoesv13en.dtdemo.ru/#/en/1824⟩ (accessed 18.03.15).
Schaber, K., Steinke, F., Hamache, T., 2012. Transmission grid extensions for the integration of variable renewable energies in Europe: who benefits where? Energy Policy 43, 123–135.
SGCC, 2014. Official. [Online] Available at: ⟨http://www.sgcc.com.cn/xwzx/gsxw/2014/09/309866.shtml⟩ (accessed 30.06.15).
Shinoda, K., 2013. Coal Information in China (28 March 2013). [Online] Available at: ⟨http://coal.jogmec.go.jp/info/docs/report_130328_17.pdf⟩ (accessed 13.03.15) (in Japanese).
Shiraki, H., Kameyama, Y., Moriguchi, Y., Hashimoto, S., 2011. Simulation analysis of renewable energy installation scenarios in Japan's Electricity Sector in 2020 using a multi-regional optimal generation planning model. J. Jpn. Soc. Energy Resour. 33, 1 (in Japanese).
Skoltech, 2015. The Study of Northeast Asia Supergrid and Exchange of Electricity Intensive Services in the Region. Presentation material at the second international workshop on the Asian energy supergrid project, Moscow, 3 April, 2015. ⟨http://crei.skoltech.ru/energysystems/news-2/⟩).
Smirnov, V.V., 2012. The perspectives of Expanding Cooperation between Russia and China in the Electric Power Industry, Irkutsk: Presentation Material at AEC-2012, Russia.
SO UPS, 2014b. 2014 Annual report of SO-UPS. [Online] Available at: ⟨http://www.so-ups.ru/fileadmin/files/company/reports/disclosure/2015/ups_rep2014.pdf⟩ (accessed 04.08.15) (in Russian).
SO UPS, 2014. Generation and consumption (per hour) - SO-UPS website. [Online] Available at: ⟨http://www.so-cdu.ru/⟩ (accessed 30.11.14) (in Russian).
Streets, D., 2003. Environmental benefits of electricity grid interconnections in Northeast Asia. Energy 28, 789–807.
TEPCO, 2013. Electricity Demand and Supply in 2013 Summer. Tokyo Electric Power Company, Tokyo.
TEPCO, 2014. Tokyo Electric Power Company: Action plan for FY 2014. [Online] Available at: ⟨http://www.tepco.co.jp/ir/tekiji/pdf/140331-1.pdf⟩ (accessed 30.06.15) (in Japanese).
Yun, W.-C., Zhang, Z.X., 2006. Electic power grid interconnection in Northeast Asia. Energy Policy 34, 2298–2309.
Yoon, J., 2007. Possible Interconnection Scenarios and impacts on composite system reliability between ROK, DPRK and RF. Presentation Material at IEEE RES 2007 General Meeting.
Zhao, M., Zhizhang, L., Qingzhu, Z., 2009. Testing and analyzing of solar energy resource assessment in Inner Mongolia. In: Proceedings of IEEE ICIEA 2009, Xi'an.